Journal of Medicinal Chemistry

pubs.acs.org/jmc

Article

# Novel Aryl Sulfonamide Derivatives as NLRP3 Inflammasome Inhibitors for the Potential Treatment of Cancer

Valentina Albanese,[▽] Sonia Missiroli,[▽] Mariasole Perrone,[▽] Martina Fabbri, Caterina Boncompagni, Salvatore Pacifico, Tiziano De Ventura, Antonella Ciancetta, Giulio Dondio, Franz Kricek, Paolo Pinton, Remo Guerrini, Delia Preti,* and Carlotta Giorgi*

Cite This: https://doi.org/10.1021/acs.jmedchem.3c00175

Read Online

ACCESS | Metrics & More | Article Recommendations | Supporting Information

**ABSTRACT:** The NLRP3 inflammasome is a critical component of innate immunity that senses diverse pathogen- and host-derived molecules. However, its aberrant activation has been associated with the pathogenesis of multiple diseases, including cancer. In this study, we designed and synthesized a series of aryl sulfonamide derivatives (ASDs) to inhibit the NLRP3 inflammasome. Among these, compounds **6c**, **7n**, and **10** specifically inhibited NLRP3 activation at nanomolar concentrations without affecting the activation of the NLRC4 and AIM2 inflammasomes. Furthermore, we demonstrated that these compounds reduce interleukin-1$\beta$ (IL-1$\beta$) production *in vivo* and attenuate melanoma tumor growth. Moreover, metabolic stability in liver microsomes of **6c**, **7n**, and **10** was studied along with plasma exposure in mice of the most interesting compound **6c**. Therefore, we generated potent NLRP3 inflammasome inhibitors, which can be considered in future medicinal chemistry and pharmacological studies aimed at developing a new therapeutic approach for NLRP3 inflammasome-driven cancer.

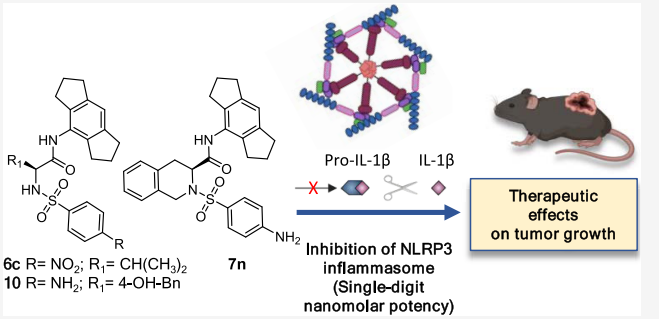




## INTRODUCTION

The NLRP3 inflammasome is a multimeric protein complex formed by Nod-like receptor family protein containing a pyrin domain 3 (NLRP3), the adaptor apoptosis-associated speck-like protein (ASC), and the effector pro-caspase 1. Once activated, NLRP3 oligomerizes and interacts with ASC through its N-terminal pyrin domain (PYD), and then, ASC recruits and binds pro-caspase-1 via their shared domain CARD (caspase activation and recruitment domain), inducing autoproteolytic caspase-1 activation. Caspase-1, in turn, induces the maturation and release of the inflammatory cytokines interleukin-1beta (IL-1$\beta$) and interleukin-18 (IL-18).[1]

NLRP3 inflammasome activation requires two steps, priming, and activation, to exert its biological effects.[2] The priming step is provided by inflammatory stimuli that involve Toll-like receptors (TLRs), which induce NFKB-mediated NLRP3 and pro-IL-1$\beta$ expression and post-translational modifications of NLRP3. The activation step is triggered by exposure to damage-associated molecular patterns (DAMPs) and pathogen-associated molecular patterns (PAMPs) or other stimuli that promote NLRP3 inflammasome assembly and the final release of IL-1$\beta$ and IL-18.[3]

The NLRP3 inflammasome has been associated with several inflammatory-based pathologies, including neurodegenerative and metabolic diseases, atherosclerosis, and cancer. The role of the NLRP3 inflammasome in the regulation of cancer has attracted increased attention in recent years, and research has identified a complex scenario in which NLRP3 acts as a double-edged sword.[4] However, the clinical relevance of the NLRP3 inflammasome in the different phases of tumorigenesis may lead to a potential strategy for the development of novel anticancer therapies.

These findings prompted the development of potent and selective NLRP3 inhibitors that are extensively used as pharmacological tools to elucidate possible clinical applications of NLRP3 targeting strategies.[5,6] In this rapidly expanding research field, numerous compounds are already under preclinical investigation, and few of them have reached phase I/II clinical trials.[7−11] Among these, MCC950 (**1**, Figure 1) is the most studied NLRP3 inhibitor after its early discovery in 2003.[12] MCC950 was shown to block canonical and non-canonical NLRP3 activation at nanomolar concentrations *in vitro* with high selectivity over AIM2, NLRC4, or NLRP1 inflammasomes.[13] Recent studies have demonstrated that the molecule reversibly binds NLRP3 at/or in the proximity of the

**Received:** January 31, 2023

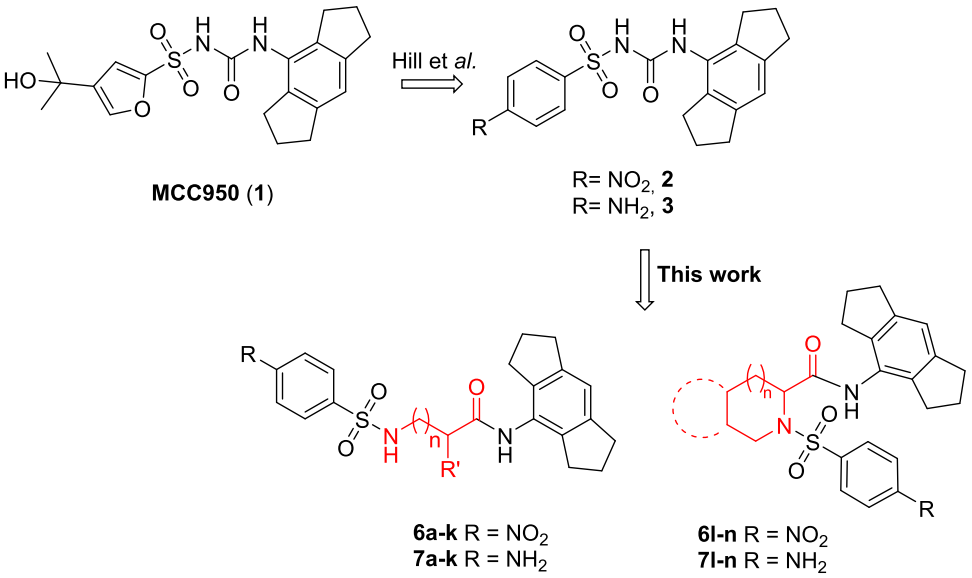


**Figure 1.** Rational design of the newly synthesized compounds starting from the known NLRP3 inhibitor MCC950.

Walker B motif of the NACTH domain, preventing NLRP3-mediated ATP to ADP hydrolysis.[14,15] In preclinical studies, the compound exhibited efficacy in different *in vivo* models with good oral bioavailability and reached a phase II clinical trial for the potential treatment of rheumatoid arthritis. However, the study was discontinued since the molecule seemed to induce an elevation of serum liver enzyme levels for reasons that are still unclear.[16] In cancer treatment, MCC950 was shown to suppress cell proliferation in chronic myeloid leukemia[17] and pancreatic adenocarcinoma[18] and to delay tumor growth in a head and neck squamous cell carcinoma mouse model.[19]

In this work, we synthesized and biologically evaluated a novel series of aryl sulfonamide derivatives (ASDs) that were designed as NLRP3 inhibitors given the available structure−activity relationship (SAR) information on MCC950. All of the molecules were evaluated *in vitro*, leading to the identification of three compounds that exhibited potent activity in inhibiting IL-1$\beta$ release by macrophages and affecting the activation of the NLRP3 inflammasome. Molecular docking studies based on the NLRP3 cryogenic electron microscopy (cryo-EM) structure, by implementing the knowledge available on MCC950 binding at the time we performed the analysis, suggested a consensus binding mode for the new analogues consistent with the observed SAR trends and supported a specific interaction of ASDs with NLRP3. The most potent inhibitors *in vitro* were further investigated for their activity *ex vivo* and *in vivo* along with *in vitro* metabolic stability in liver microsomes. Finally, given the involvement of the NLRP3 inflammasome in the pathophysiology of cancer, we used a cancer mouse model to verify the efficacy of these new compounds in terms of tumor growth reduction. Our *in vivo* studies confirmed the ability of the selected molecules to dampen tumor growth after intraperitoneal administration. In particular, compound **6c** also showed good plasma exposure when intraperitoneally administered in mice.

## RESULTS

**Design and Synthesis of Novel NLRP3 Inhibitors.** For the identification of a new class of small-molecule NLRP3 inhibitors, the available SAR information around MCC950 has been first taken into account. The structure of MCC950 (**1**, Figure 1) is characterized by a sulfonylurea core linking a 4-(2-hydroxypropan-2-yl)furan-2-yl moiety to a 1,2,3,5,6,7-hexahydro-s-indacen-4-yl tricyclic system. The furan portion of MCC950 is not mandatory for promoting NLRP3 blockade, as demonstrated recently by Hill et al. with the synthesis of analogues **2** and **3** (Figure 1), which were shown to maintain nanomolar potency *in vitro*.[20] Other studies demonstrated that limited modifications of the indacenamine nucleus seem to be tolerated.[21] In particular, molecular dynamic simulations highlighted the importance of the central aromatic ring of this portion of MCC950 that would be involved in the $\pi-\pi$ stacking interaction with F257 and F304 of the NLRP3 Walker B site.[15]

Given that sulfonylurea drugs such as glyburide are used therapeutically for the treatment of type 2 diabetes,[22] the structure of MCC950 was recently modified for the development of dual-acting molecules able to inhibit NLRP3-induced IL-1$\beta$ release and to stimulate insulin secretion.[20] This approach was considered to treat pathologies linked to pancreatic $\beta$-cell death and multiple inflammatory complications of type 2 diabetes. However, these kinds of ligands are not useful for indications other than diabetes, as they could increase the risk of hypoglycemia.

Given this information, herein, we report the development of a novel series of NLRP3 small-molecule inhibitors in which the sulfonylurea of MCC950 was modified through the interposition of different linear or cyclic $\alpha/\beta$ amino acids between the hexahydro-s-indacen-4-amine moiety and the sulfone functions (Figure 1). In particular, we explored the effect of the introduction of both proteinogenic and nonproteinogenic amino acids with aliphatic, branched, aromatic, or polar side chains. This modification was supposed to retain NLRP3 inhibitory activity while removing the typical sulfonylurea function that can exert hypoglycemic effects. In this SAR study, the indacenamine portion will be maintained, whereas *p*-nitro or *p*-aminophenyl moieties will replace the furan ring of MCC950 analogously to **2** and **3**. The latter substitution increased the synthetic accessibility of the target compounds; moreover, the removal of the furan portion could possibly address the liver toxicity issues since 2-unsubstituted furan rings are known to lead to unstable hepatotoxic metabolites.[23]


https://doi.org/10.1021/acs.jmedchem.3c00175
J. Med. Chem. XXXX, XXX, XXX−XXX

**Scheme 1. Synthesis of the Final Compounds 6/7a−h, 6−7k, and 8−11**[a]

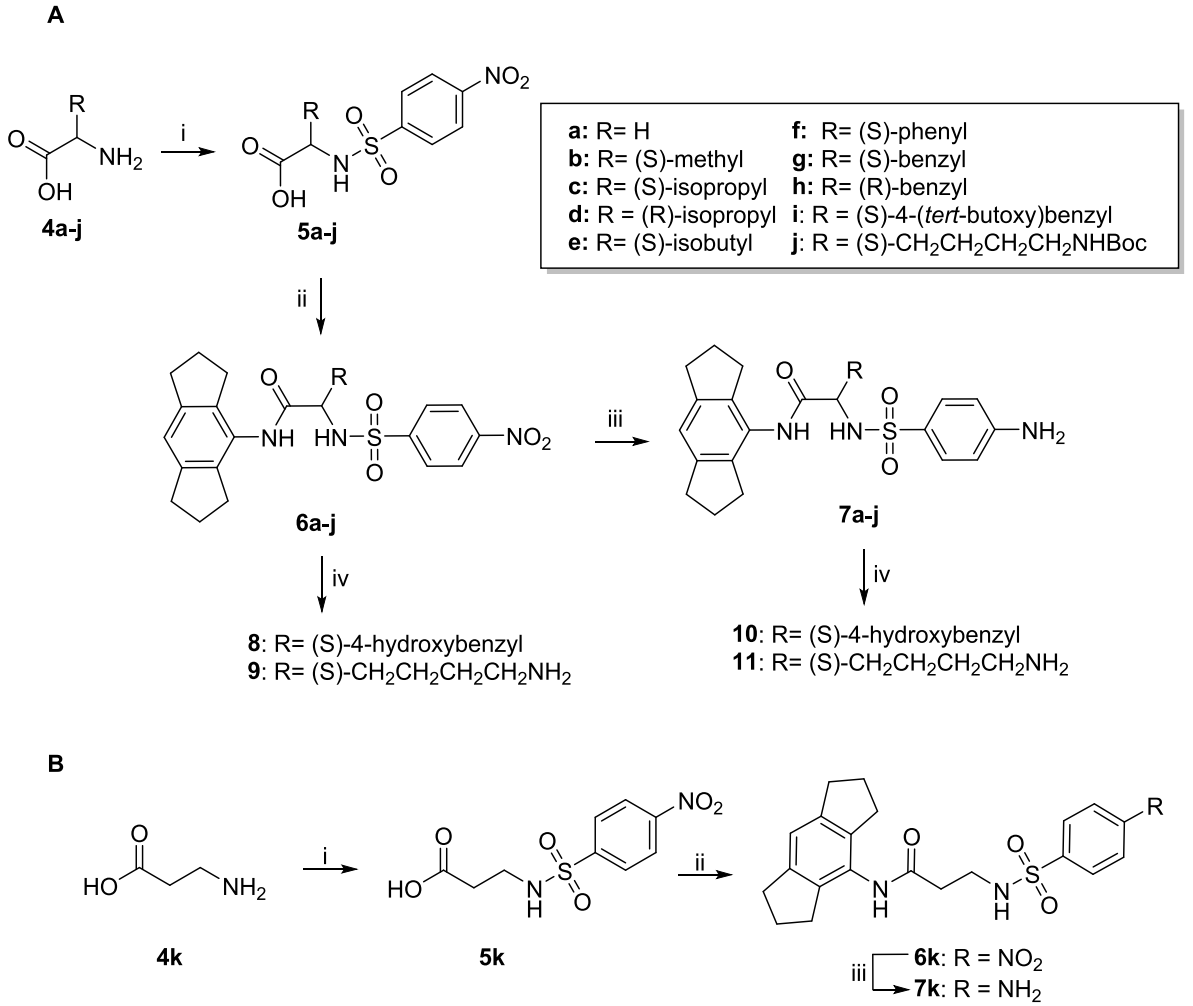


[a]Reagents and conditions: (i) 4-Nitrobenzenesulfonyl chloride, $NaHCO_3$, $H_2O$, r.t., 16 h; (ii) Hexahydro-s-indacen-4-amine, HATU, DIPEA, DMF, 0 °C to r.t., 2−5 h; (iii) $H_2$ Pd/C, $CH_3COOH$, EtOAc, r.t, 16 h; (iv) 4N HCl in dioxane, 2 h.

**Scheme 2. Synthesis of the Final Compounds 6l−n and 7l−n**[a]

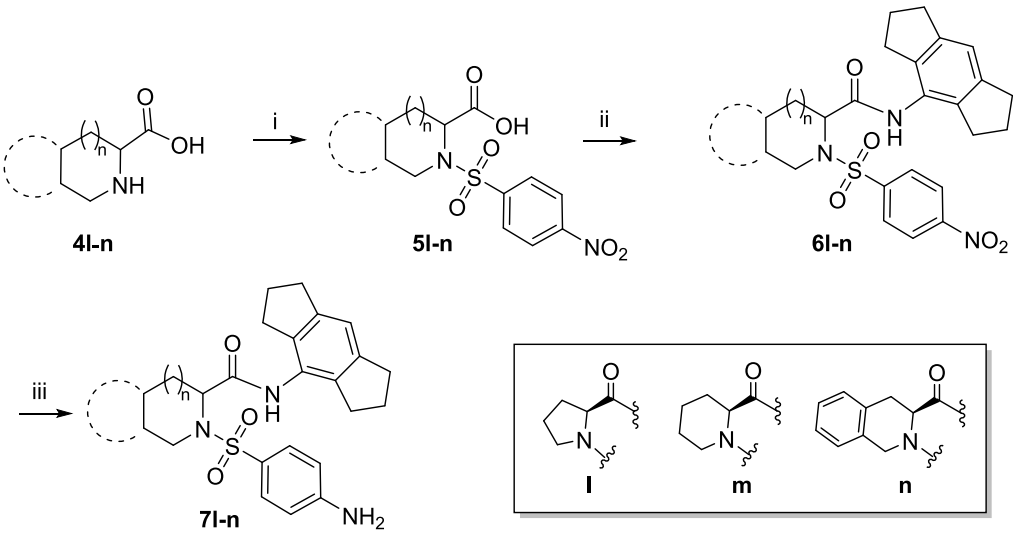


[a]Reagents and conditions: (i) 4-Nitrobenzenesulfonyl chloride, $NaHCO_3$, $H_2O$, r.t., 16 h; (ii) Hexahydro-s-indacen-4-amine, HATU, DIPEA, DMF, 0 °C to r.t., 2−5 h; (iii) $H_2$ Pd/C, $CH_3COOH$, EtOAc, r.t, 16 h.


https://doi.org/10.1021/acs.jmedchem.3c00175
J. Med. Chem. XXXX, XXX, XXX−XXX

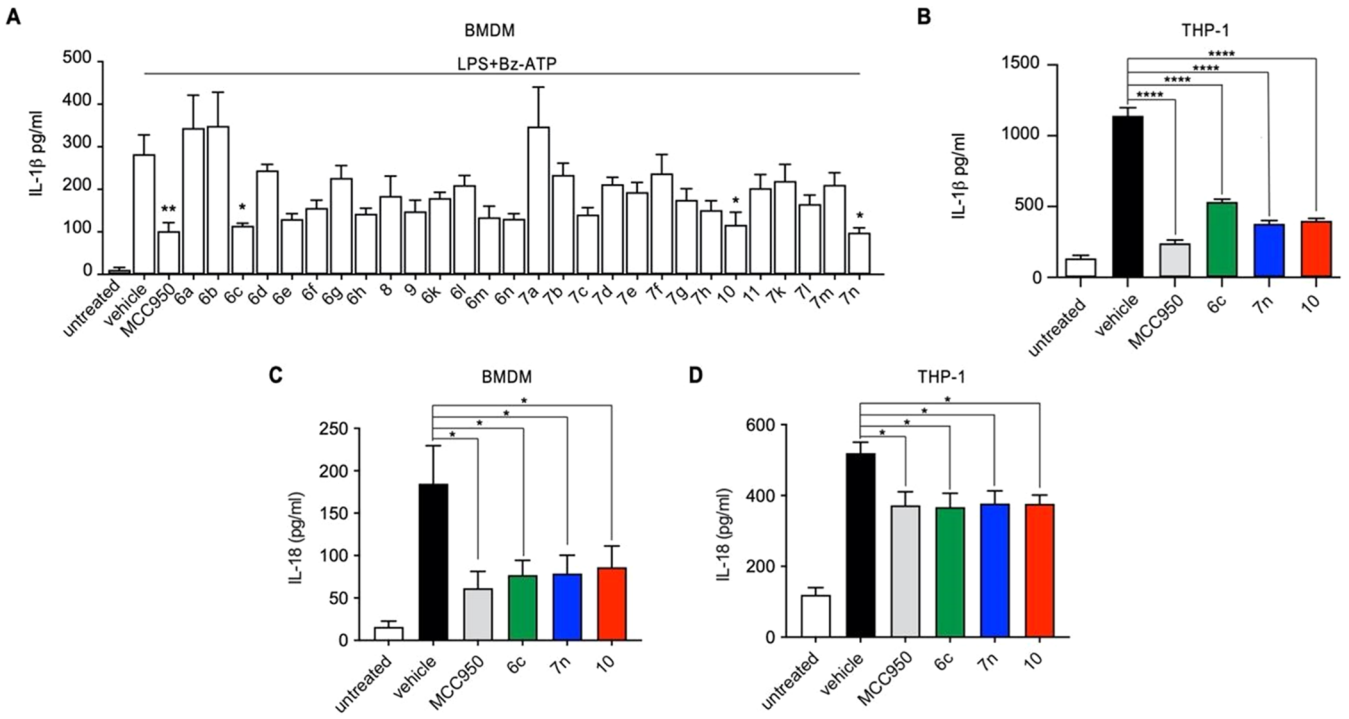


**Figure 2.** Compounds **6c**, **7n**, and **10** inhibit the NLRP3 inflammasome activation. (A) ELISA of IL-1$\beta$ in supernatant from BMDM cells treated with LPS, the novel ASDs (1 $\mu$M), and stimulated with Bz-ATP. (B) ELISA of IL-1$\beta$ in supernatant from LPS-primed THP-1 cells treated with the novel ASDs (1 $\mu$M) and stimulated with ATP. (C, D) Production of IL-18 from BMDM (C) and THP-1 cells (D) stimulated with LPS and ATP and treated with ASDs (1 $\mu$M) measured by ELISA. Bars: S.E.M. *$p < 0.05$, **$p < 0.01$, ****$p < 0.0001$.

All of the tested inhibitors were obtained through a straightforward and low-cost synthetic approach of three/four steps with high total yields (64−84%). As depicted in Scheme 1, commercially available $\alpha/\beta$ amino acids (**4a**−**k**) were employed as starting reagents for the synthesis of the linear sulfonamide derivatives **6a**−**h**, **7a**−**h**, **6**−**7k**, and **8**−**11**. All of the starting amino acids were used as unprotected molecules except in the case of target compounds **8**−**11**, which required proper protection of the side chain functional groups of tyrosine and lysine [H-Tyr(tBu)-OH and H-Lys(Boc)-OH].

Regioselective sulfonation of the alfa amino group was performed by a first reaction with 4-nitrobenzenesulfonyl chloride in the presence of sodium hydrogen carbonate to give the sulfonamide derivatives **5a**−**k**. The subsequent HATU-mediated coupling with hexahydro-s-indacen-4-amine in the presence of DIPEA afforded the nitro derivatives **6a**−**k**. Hexahydro-s-indacen-4-amine was synthesized as previously reported.[24] The tyrosine (**6i**) and lysine (**6j**) derivatives were treated in acidic conditions to remove side chain protections giving the final compounds **8** and **9**. Compounds **6a**−**k** were reduced to the corresponding amino derivatives by hydrogenation using 10% palladium on a carbon catalyst to give compounds **7a**−**k**. The side chain protections of the 4-$NH_2$-phenyl sulfonamides **7i**−**j** were cleaved by acid treatment to provide compounds **10** and **11**. The final cyclic analogues **6l**−**n** and **7l**−**n** were obtained by a similar approach starting from proline, pipecolic acid, or 1,2,3,4-tetrahydroisoquinoline-3-carboxylic acid, as described in Scheme 2. HPLC analysis (Supplementary Information) showed a purity grade higher than 95% for all of the final compounds.

**ASDs Potently Inhibit NLRP3-Mediated Release of IL-1$\beta$ *In Vitro*.** The *in vitro* activity of all of the synthesized compounds was evaluated by testing their effects on the release of IL-1$\beta$ as readout of NLRP3 inflammasome activation. Mouse bone marrow-derived macrophages (BMDMs) were first primed with 1 $\mu$g/ml lipopolysaccharide (LPS) from *Escherichia coli*, treated with the novel ASDs at a concentration of 1 $\mu$M, and finally stimulated with 2′(3′)-O-(4-benzoylbenzoyl)adenosine 5′-triphosphate triethylammonium salt (Bz-ATP). Cell culture supernatants were analyzed for IL-1$\beta$ by enzyme-linked immunosorbent assays (ELISAs), revealing that compounds **6c**, **7n**, and **10** exhibited desirable inhibitory activity (Figure 2A). The percent inhibition of IL-1$\beta$ production (I %) is reported for each inhibitor in Table 1. MCC950, chosen as an internal reference, displayed 63.9% inhibition of the release of IL-1$\beta$ under the same conditions.

In most cases, the novel modification of the sulfonylurea core through the interposition of different amino acids between the hexahydro-s-indacen-4-amine moiety and the sulfone functions was demonstrated to be effective in preserving the inhibitory activity. However, the chemical nature of the side chain of the introduced amino acid significantly affected the potency of the investigated analogues. A complete loss of activity was observed when a glycine residue was introduced (compounds **6a** and **7a**), while the introduction of branched alkyl side chains led to a marked enhancement of activity, such as for compounds **6c**, **7c**, and **6e**. Aromatic residues were also generally well tolerated (see in particular the phenylglycine derivative **6f** and the phenylalanine derivative **7g**). Interestingly, the tyrosine derivatives **8** and **10** exhibited a significantly higher potency in preventing IL-1$\beta$ production than the corresponding phenylalanine congeners **6g** and **7g**. The introduction of polar residues was also explored with derivatives **9** and **11**, and good results were obtained by combining a 4-$NO_2$ phenyl sulfonamide moiety with lysine.

With the synthesis of **6k** and **7k**, we wanted to estimate the effect of a longer spacer between the amide carbonyl and the


https://doi.org/10.1021/acs.jmedchem.3c00175
J. Med. Chem. XXXX, XXX, XXX−XXX

**Table 1. Inhibitory Activity of All of the Synthesized Compounds Measured by ELISA**

| compd | inhibitory rates of IL-1$\beta$ (%)[a] | compd | inhibitory rates of IL-1$\beta$ (%)[a] |
|---|---|---|---|
| **vehicle** | 0 (282.99 ± 45.14) | | |
| **MCC950** | 63.9 (102.06 ± 20.10) | | |
| **6a** | inactive (344.01 ± 79.93) | **7a** | inactive (347.97 ± 92.70) |
| **6b** | inactive (349.16 ± 78.94) | **7b** | 17.3 (233.94 ± 27.88) |
| **6c** | 59.4 (114.97 ± 5.62) | **7c** | 50.2 (140.94 ±16.08) |
| **6d** | 13.5 (244.83 ± 13.70) | **7d** | 25.1 (211.91 ± 16.58) |
| **6e** | 53.9 (130.51 ± 12.52) | **7e** | 31.5 (193.91 ± 22.80) |
| **6f** | 44.8 (156.32 ± 18.28) | **7f** | 16.1 (237.40 ± 44.91) |
| **6g** | 19.8 (227.08 ± 29.16) | **7g** | 38.0 (175.41 ± 26.35) |
| **6h** | 49.5 (142.78 ± 12.79) | **7h** | 46.4 (151.58 ± 21.95) |
| **8** | 34.7 (184.91 ± 46.23) | **10** | 58.8 (116.73 ± 29.96) |
| **9** | 47.5 (148.65 ± 26.00) | **11** | 28.4 (202.70 ± 32.43) |
| **6k** | 36.5 (179.59 ± 13.74) | **7k** | 22.3 (219.98 ± 38.99) |
| **6l** | 25.7 (210.27 ± 22.44) | **7l** | 41.6 (165.27 ± 21.87) |
| **6m** | 52.4 (134.81 ± 25.88) | **7m** | 25.4 (211.00 ± 28.31) |
| **6n** | 53.7 (131.08 ± 11.72) | **7n** | 65.2 (98.47 ± 11.16) |

[a]ELISA analysis of IL-1$\beta$ in cell culture supernatant from BMDMs stimulated with LPS, various compounds at dose 1 $\mu$M and then treated with Bz-ATP. MCC950 served as positive control. All data were expressed as mean ± SEM of three independent experiments carried out in triplicate. Values in parentheses refer to the quantity of IL-1$\beta$ expressed in pg/mL.

sulfonamide nitrogen. In this case, the flexible unsubstituted ethylene spacer derived from $\beta$ alanine was more effective in promoting NLRP3 inhibition than the methylene linker of the glycine derivatives **6a** and **7a**.

Our SAR analysis was extended to some examples of constrained analogues that were obtained from proteinogenic or nonproteinogenic cyclic amino acids such as proline (**6**−**7l**), pipecolic acid (**6**−**7m**), and 1,2,3,4-tetrahydroisoquinoline-3-carboxylic acid (**6**−**7n**). Excellent results were obtained with the isoquinoline derivatives **6n** and **7n**. In particular, compound **7n** was identified as the most potent NLRP3 inhibitor discovered herein, with an I % against LPS/Bz-ATP-induced IL-1$\beta$ release comparable to that of MCC950. Among the investigated compounds, we did not observe a clear preference for the 4-$NO_2$ or the 4-$NH_2$ group on the phenyl sulfonamide moiety. Indeed, the relative potency of the $NO_2$ derivatives (**6a**−**n**, **8**, and **9**) compared with the corresponding $NH_2$ congeners (**7a**−**n**, **10**, and **11**) is largely dependent on the nature of the spacer side chain.

Most of the newly reported compounds were synthesized from amino acids with an L-configuration. To investigate possible stereoselective recognition by the biological target, we synthesized both the R and S enantiomers of the valine and phenylalanine derivatives. We observed a significant preference for the L-configuration in the case of valine substitution (compare **6c**−**d** and **7c**−**d** in Table 1). However, this trend was not confirmed with the phenylalanine analogues in which the R isomer was favored in the presence of the 4-$NO_2$-phenyl group (compare **6g** and **6h**) while, when the $NH_2$-phenyl group was introduced (compare **7g** and **7h**), we observed a comparable potency for the two stereoisomers.

To further confirm the inhibitory effect of these compounds on the NLRP3 inflammasome, we treated differentiated human THP-1 cells with LPS, selected compounds, and Bz-ATP (Figure 2B); MCC950 served as a positive control, while DMSO served as vehicle control. The data revealed the inhibitory effects of compounds **6c**, **7n**, and **10** in human macrophages (Figure 2B). Accordingly, the NLRP3-stimulated secretion of IL-18 was also significantly reduced after treatment with compounds **6c**, **7n**, and **10** both in BMDM and THP-1 cells (Figure 2C,D).

**Molecular Docking and SPR Analysis Support a Specific Interaction of ASDs with NLRP3.** Newly synthesized analogues were docked at a homology model based on the cryo-EM structure of the inactive human (h) NLPR3 in complex with ADP and NEK7 (PDB ID: 6NPY) by centering the search on *Site 3* (Figure 3A), corresponding to the recently identified MCC950 binding site.[25] Although the functional data *in vitro* were obtained with the mouse (m) NLPR3 (Table 1), the high sequence conservation of the NACHT domain (87.7% and 92.1% sequence identity and similarity, respectively) and, in particular, the identical composition of Walker A and B motifs in the human and mouse isoforms indicates that the modeling at the hNLPR3 is predictive of mNLPR3 binding.

Based on the structural similarity of the new analogues to the reference compound, we assumed that they bind in the same region. As the coordinates of the MCC950-hNLPR3 complex were not available at the time we performed the analysis, we evaluated the ability of the induced fit docking (IFD) protocol to qualitatively reproduce the binding mode reported in the description accompanying the cryo-EM data.[25] The IFD procedure returned docking poses with a consistent orientation corresponding to the experimentally observed MCC950 binding mode and featuring slightly different interaction patterns among each other, as highlighted in Figure 3B,C. MCC950 binds at the interface of four domains with residues in the HD1 and WHD domains, forming a hydrophobic spot with the hexahydro-s-indacen-4-amine moiety, the NBD domain anchoring the acyl-sulfonamide function to the GAA sequence of the Walker A motif, and the HB2 domain providing additional interactions stabilizing the furan head.

As depicted in Figure 3B,C, hexahydro-s-indacen-4-amine establishes hydrophobic contacts with I411, L413, and V414 in HD1. M408 (HD1, not shown) and T439 (WHD) lie behind and on top of the tricyclic system, respectively, and contribute to the overall shape of the pocket. A tight network of H-bonds anchors the acyl-sulfonamide moiety to the NBD: the MCC950 NH group and the deprotonated nitrogen atom engage the A228 backbone, and one of the sulfone oxygen atoms establishes a strong H-bond to the R351 side chain. Additional electrostatic stabilization is provided by the acyl-sulfonamide carbonyl H-bonding K567 side chain (HD2). The poses in Figure 3B,C differ for the orientation of the furan head group with two alternative interaction patterns: one featuring H-bonds between the ligand hydroxyl and E563 and Q644 side chains (HD2) and hydrophobic contacts between the methyl moiety and V353 (NBD, Pose 1 in Figure 3B), and the other mode features a $\pi$-cation interaction between the furan ring and K567 side chain (HD2, Pose 2 in Figure 3C). After the coordinates of the MCC950-hNLPR3 complex were deposited (PDB ID: 7PZC), we validated our predicted binding site location and ligand binding modes retrospectively by superimposing the modeled complexes onto the experimental structure. As shown in Figure S1 (see the Supporting Information), our predictions show excellent agreement with the experimental data: Site 1 spheres overlap perfectly with the MCC950 surface (gray surface in Figure S1A), and the poses in Figure 3B,C have average RMSD values of 1.3 and 1.7 Å, respectively, with respect to the experimental ligand coordinates (see Figure S1B, C; cryo-EM resolution: 3.9 Å).


https://doi.org/10.1021/acs.jmedchem.3c00175
J. Med. Chem. XXXX, XXX, XXX−XXX

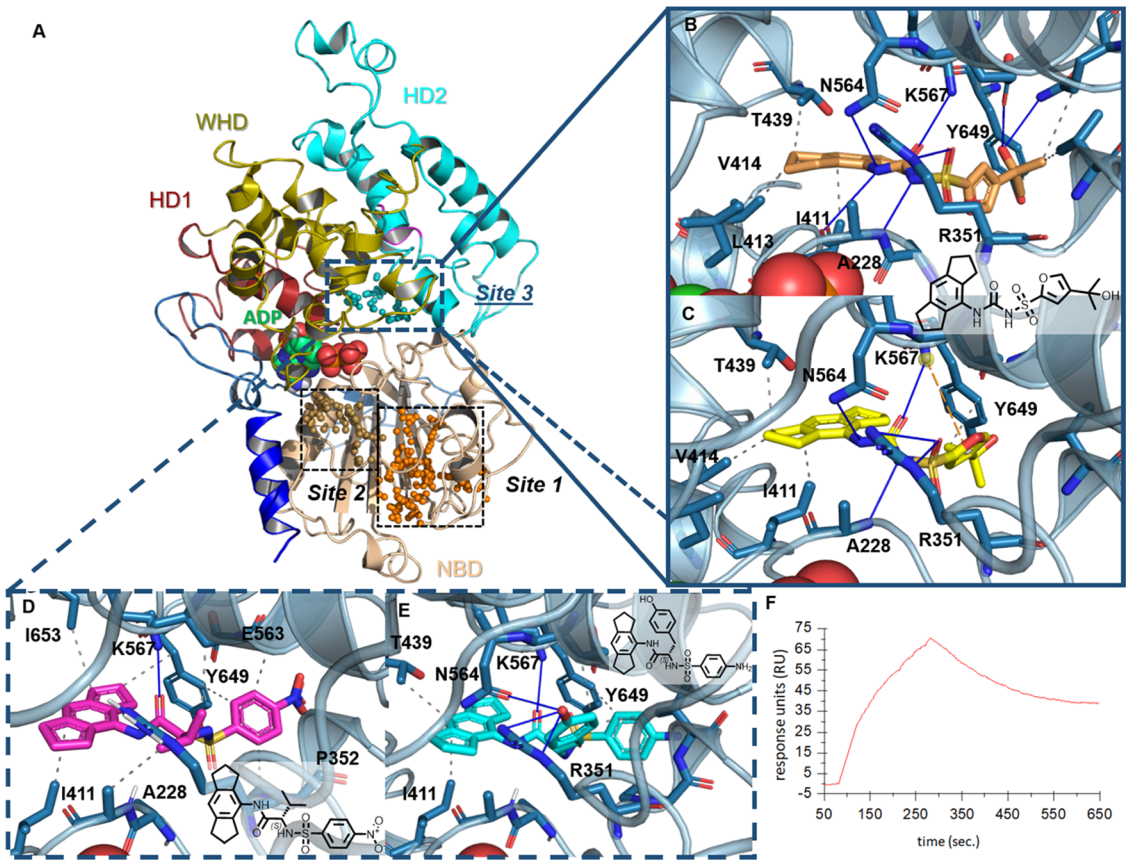


**Figure 3.** Molecular modeling of MCC950 and compounds **6c** and **10**, and SPR sensorgram of compound **10**. (A) Overall structure of hNLRP3 homology model (based on PDB ID: 6NPY template) used for docking in complex with ADP (green spheres). The five subdomains in the NACHT domain are highlighted with different colors as follows: FISNA (blue), NBD (pink), HD1 (red), WHD (yellow), HD2 (cyan); the top three putative binding sites identified by Site Finder are represented by orange, sand, and teal $\alpha$ spheres, respectively. (B−E) Predicted binding modes of selected analogues at Site 3: the ligand is represented in sticks with orange, yellow, magenta, and cyan carbon atoms for MCC950 (Pose 1), MCC950 (Pose 2), **6c**, and **10**, respectively; side chains of interacting residues are in stick representation (blue carbon atoms); H-bonds, $\pi$−cation, and hydrophobic interactions are pictured as blue solid, and orange and gray dashed lines, respectively. Hydrogen atoms are omitted. (F) SPR sensorgram showing binding of compound **10** (100 $\mu$L analyte solution) to NLRP3 ligand covalently coupled to flow cell 2 (FC2) of the SPR sensor chip surface, representing a double-referenced curve selected from duplicate runs obtained by subtraction of data generated on ligand free flow cell 1 (FC1) followed by subtraction of a zero analyte buffer sensorgram on FC2.

Based on the above-described MCC950 binding mode, the interposition of side chains between the hexahydro-s-indacen-4-ammide and the sulfone moieties is expected to impact the electrostatic interactions (*i.e.*, with R351 and K567) anchoring the (acyl-)sulfonamide that no longer features a net negative charge in the new derivatives. As highlighted in the SAR trend in Table 1, compensation for the lost electrostatic stabilization seems to be achieved with the introduction of bulky spacers that recover the activity. As illustrated by the docking pose of **6c** (Figure 3D), the isopropyl group pushes the scaffold away from the R351 (NDB) side chain while maintaining hydrophobic contacts with A228 (NDB) and the carbon atoms of the E563 (HD2) side chain. The interposition of a tyrosine side chain recovers the interaction with R351 (NDB), which H-bonds the hydroxyl moiety alongside the N564 (HD2) side chain (see the docking pose of **10** in Figure 3E). It is therefore conceivable that the additional polar interactions established by the **10** hydroxyl group account for the enhanced activity with respect to unsubstituted aromatic rings. In addition, consistent with the observed general lack of preference for the *p*-$NH_2$ or *p*-$NO_2$ group, the phenyl sulfonamide moiety in the docking poses of **6c** and **10** (Figure 3D,E) does not engage in specific interactions and is projected toward a solvent-exposed region: in such an orientation, the phenyl ring establishes hydrophobic contacts with surrounding residues in HD2 and WHD domains, namely, Y649, P352, and V353 side chains and the carbon atoms of E563 and Q644 side chains.

The above-described binding mode, however, is not applicable to analogues bearing bulky constrained linkers, such as the isoquinoline ring of **6n** and **7n**. As depicted in Figures S2A, **7n** docked with the interposed side chain and the phenyl sulfonamide moiety lying in the hydrophobic spot, and the hexahydro-s-indacen-4-amine moiety turned approximately −90° with respect to the MCC950 docking pose (Figure S2B). In this orientation, the tricyclic ring of the hexahydro-s-indacen-4-amide establishes interactions with the same hydrophobic residues as in MCC950 pose, namely, A227, A228, I411, and T439, and the amide function engages in polar interactions with K567 (HD2). The isoquinoline ring is projected toward the back of the pocket in contact with I563 and K652 in the transition leucine-rich repeat (trLRR) domain. Superimposition of the docked pose to the full cryo-EM structure (Figure S2C) reveals potential for additional interactions with hydrophobic residues in trLRR, such as V704, Q705, V706, and L708, which were not included in the model used for docking. The phenyl sulfonamide group establishes hydrophobic interactions with


https://doi.org/10.1021/acs.jmedchem.3c00175
J. Med. Chem. XXXX, XXX, XXX−XXX

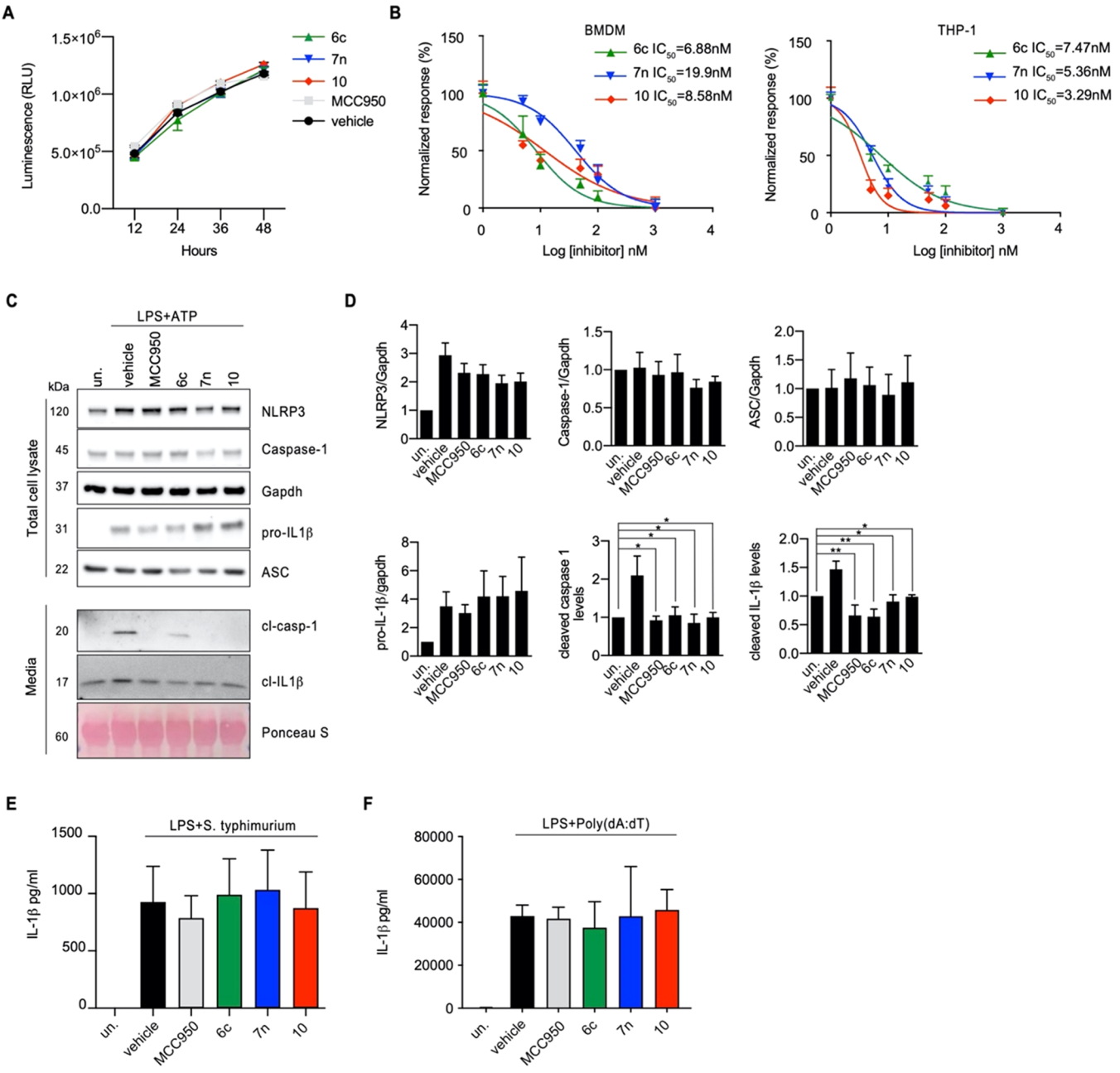


**Figure 4.** ASDs suppress caspase-1 activation and IL-1$\beta$ secretion. (A) Cell viability of THP-1 was measured with RealTime-Glo MT Cell Viability assay. Cells were treated with selected inhibitors at 1 $\mu$M and were monitored for 48 h. (B) Production of IL-1$\beta$ from BMDM and THP-1 cells stimulated with LPS and ATP and treated with compounds (1−1000 nM) as measured by ELISA. Cytokine level is normalized to that of DMSO-treated control cells. Nonlinear regression analysis was performed, and the curve of log [M] compound versus the normalized response (variable slope) is presented. All data were expressed as mean ± SEM of 3 independent experiments carried out in triplicate. (C) Culture supernatants and THP-1 cells were collected before and after LPS activation with the addition of ATP and the selected molecules. Total cell lysates (Lys) and supernatants (Sup) were resolved by SDS-PAGE. (D) Expression of NLRP3 caspase-1, pro-IL-1$\beta$, and ASC proteins normalized on GAPDH from three independent experiments. Bars: S.E.M. *$p < 0.05$, **$p < 0.01$. (E, F) Production of IL-1$\beta$ in supernatant from LPS-primed BMDMs treated with compounds **6c**, **7n**, and **10** at doses of 1 $\mu$M before transfecting with flagellin of *S. Typhimurium* (E) or with poly(dA:dT) (F).

F410 (HD1), and the *p*-$NH_2$ group engages in a H-bond with the backbone of T407 (HD1, Figure S2B). We speculate that this additional polar interaction might account for the higher affinity of **7n** for the target with respect to the *p*-$NO_2$ analogue **6n**.

The capability of our compounds to physically interact with the NLRP3 target molecule was assessed by surface plasmon resonance (SPR) analysis (Figure 3F). The positive binding signal was obtained by generating a double-referenced sensorgram, applying compound **10** as analyte binding to NLRP3 covalently attached to the surface of a Biacore optical sensor chip. The data clearly confirmed the target binding capacity of the compound.

**ASDs Selectively Inhibit NLRP3 Inflammasome Activation *In Vitro* and *In Vivo*.** Given that ELISAs revealed that compounds **6c**, **7n**, and **10** exhibited desirable inhibitory activity against the NLRP3 inflammasome, we evaluated their cytotoxicity. Our results demonstrate that the compounds did


https://doi.org/10.1021/acs.jmedchem.3c00175
J. Med. Chem. XXXX, XXX, XXX−XXX

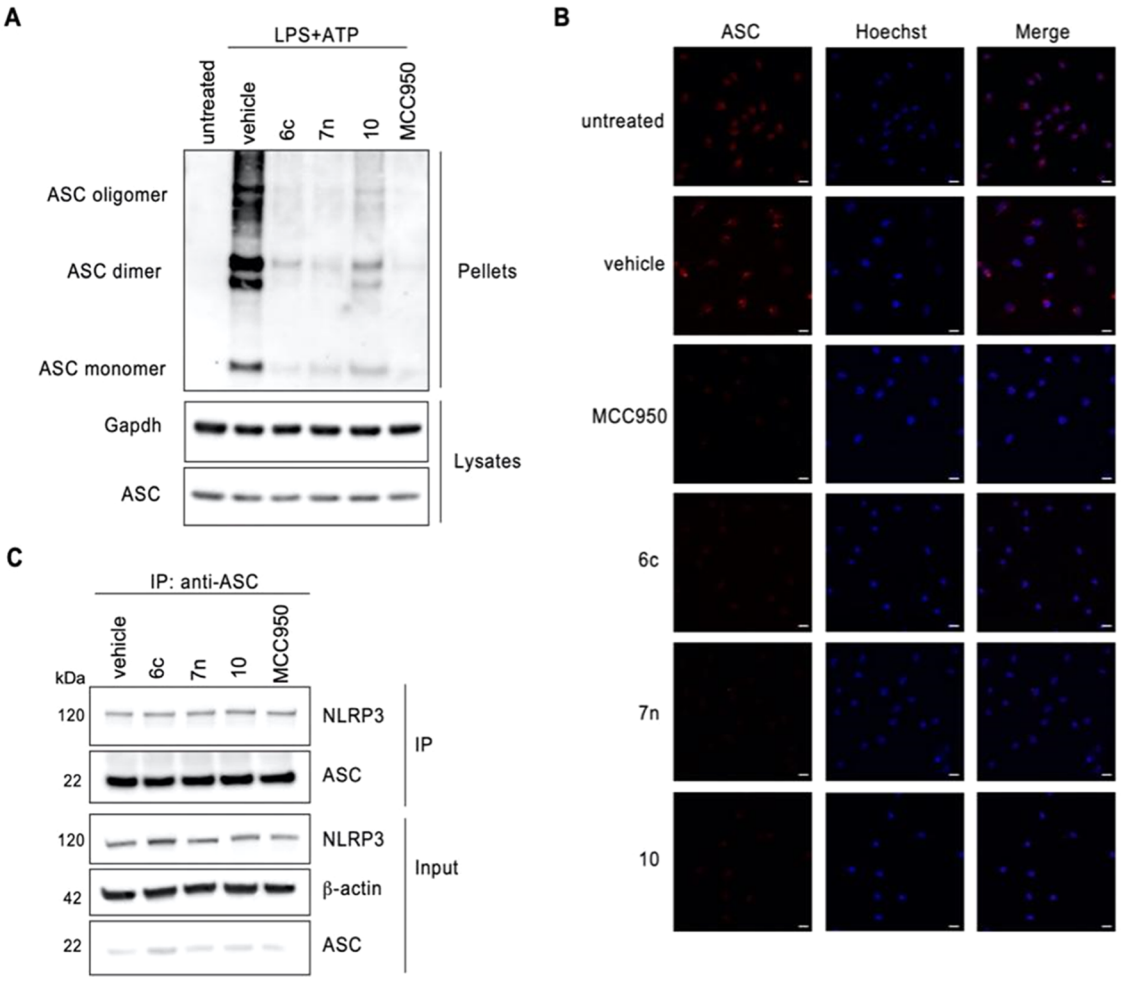


**Figure 5.** ASDs block NLRP3 inflammasome-related ASC oligomerization. (A) LPS-primed cells were treated with the novel ASDs (1 $\mu$M) and stimulated with ATP for 1 h. The cell lysates and the pellets were collected and used to analyze ASC oligomerization by western blotting. (B) BMDMs were treated as (A) were fixed with 4% paraformaldehyde followed by ASC and Hoechst staining. Scale bars: 25 $\mu$m (C) Co-IP and western blots of the interaction of ASC and NLRP3 in BMDMs stimulated with LPS (2 h), treated with ASDs (1 $\mu$M 30 min), and stimulated with ATP for 1 h. The results presented are representative of three independent experiments.

not exhibit cytotoxicity in THP-1 cells (Figure 4A). Furthermore, we measured the $IC_{50}$ values of the selected compounds by testing their effects on the release of IL-1$\beta$ from BMDM and THP-1 cells stimulated with LPS and ATP. Compounds **6c**, **7n**, and **10** displayed low nanomolar potency in both models (Figure 4B). Of note, in THP-1 cells, the isoquinoline derivative **7n** ($IC_{50}$ = 5.36 nM) and the tyrosine derivative **10** ($IC_{50}$ = 3.29 nM) were shown to be even more potent than the positive control MCC950 ($IC_{50}$: 8.1 nM in human monocyte-derived macrophages as reported in ref 9).

We next tested whether these compounds could suppress the upstream signaling of the NLRP3 inflammasome. Treatment with these compounds did not consistently affect the priming phase of NLRP3 inflammasome activation and did not alter the expression of NLRP3, caspase-1, ASC, or pro-IL-1$\beta$ in whole-cell lysates (Figure 4C,D). Interestingly, the amount of caspase-1 p10 and the processing of IL-1$\beta$ were reduced by compounds **6c**, **7n**, and **10** (Figure 4C,D).

To confirm the specific inhibitory effect of these compounds on the NLRP3 inflammasome, we also investigated whether they could inhibit the activation of other inflammasomes, such as NOD-like receptor family CARD-containing 4 (NLRC4) and absent in melanoma 2 (AIM2) inflammasomes, also responsible for the IL-1$\beta$ production. Our results showed that compounds **6c**, **7n**, and **10** had no effect on the NLRC4 inflammasome activation triggered in BMDMs by the flagellin of *Salmonella typhimurium* transfection (Figure 4E). We thus examined the effect of the same compounds on the non-NLR AIM2 inflammasome by transfecting BMDMs with the dsDNS analogue Poly (dA:dT). As reported in Figure 4F, we did not observe any reduction in the amount of IL-1$\beta$ secretion by our compounds.

Taken together, these *in vitro* data suggest that the newly designed analogues are potent and specific inhibitors of the NLRP3 inflammasome as well as MCC950.

We next examined the formation of NLRP3-dependent ASC oligomers, a key event in NLRP3 inflammasome activation. We tested whether our compounds have any effect on the ATP-induced ASC specks formation and used MCC950 as a positive control. BMDMs were treated with LPS, our compounds, and then stimulated with ATP. Once ATP triggered NLRP3 activation, the formation of ASC oligomerization was observed by western blotting and immunofluorescence (Figure 5A,B). The data showed that compounds **6c**, **7n**, and **10** attenuated the ASC-complex formation, without affecting the ASC levels in cell lysates (Figure 5A,B).


https://doi.org/10.1021/acs.jmedchem.3c00175
J. Med. Chem. XXXX, XXX, XXX−XXX

We also evaluated the effect of our compounds **6c**, **7n**, and **10** on the NLRP3-ASC interaction, which is critical for NLRP3 inflammasome assembly. Experimental results in BMDMs demonstrated that compounds **6c**, **7n**, and **10**, at a concentration of 1 $\mu$M, did not alter the interaction between NLRP3 with ASC (Figure 5C). The above results suggest that our compounds do not prevent NLRP3 inflammasome formation but rather they block its activation.

Analysis of the overall data, together with synthetic considerations, prompted us to choose compounds **6c**, **7n**, and **10** for further *in vivo* studies.

To explore the anti-inflammatory activity of these compounds *in vivo*, we adopted an LPS-induced inflammation treatment. Mice were pretreated with compounds **6c**, **7n**, and **10** or vehicle at 25 mg/kg by intraperitoneal (IP) administration for 30 min, and then intraperitoneally injected with LPS. After 4 h, peritoneal exudate and mouse plasma were collected and used to evaluate IL-1$\beta$ release. The mice that received pretreatment with the compounds displayed a strong reduction in IL-1$\beta$ production in both peritoneal exudate and blood samples (Figure 6A,B).

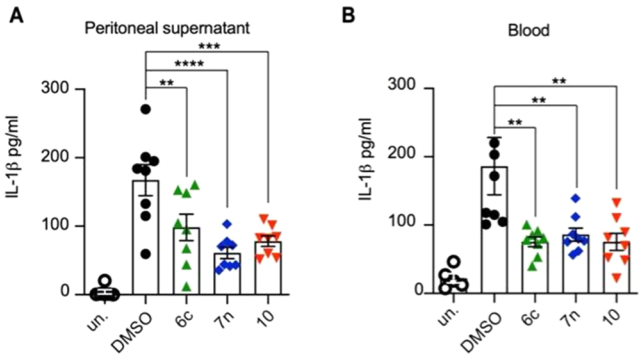


**Figure 6.** ASDs inhibit *in vivo* NLRP3 inflammasome activation. ELISA of the peritoneal exudate (A) and blood (B) levels of IL-1$\beta$ in C57BL/6 mice pretreated with compounds **6c**, **7n**, and **10** (20 mg/kg) or the vehicle control for 30 min and then treated with LPS (1 mg/kg) via IP injection for 4 h. Data were presented as mean ± SEM from three independent experiments. $^{**}p < 0.01$, $^{***}p < 0.001$, $^{****}p < 0.0001$.

Collectively, these results revealed that compounds **6c**, **7n**, and **10** exert a potent protective effect in LPS-induced treatment by inhibiting the activation of the NLRP3 inflammasome.

**Specifically Targeting NLRP3 in ASDs Reduces Tumor Growth.** NLRP3-dependent inflammation provides a more permissive environment for tumor proliferation.[4,26] In particular, NLRP3 activation and the subsequent formation of the NLRP3 inflammasome were recently shown to be involved in melanoma progression.[27] Thus, we next evaluated the effect of NLRP3 inhibition *in vivo* in a mouse cancer model. For a tumor model, we subcutaneously inoculated C57BL/6 mice with native B16-F10 melanoma cells stably transfected with a cytosolic luciferase (cytluc) construct to allow *in vivo* tumor progression monitoring. After 5 days, randomly chosen mice were subjected to IP injection of vehicle or selected molecules (thrice weekly at 25 mg/kg). At post-injection day 14, tumor masses were excised, and the **6c**-, **7n**-, and **10**-treated mice displayed tumor masses that were 2- to 3-fold smaller than those of the controls (vehicle) (Figure 7A−C).

Bioluminescence analysis allowed tumor detection and correlated with the effective tumor size measured by calipers (Figure 7D). Interestingly, we found no alteration in the expression of NLRP3, caspase-1 (total and cleaved), ASC, or pro-IL-1$\beta$ in tumor lysates (Figure 7E).

Notably, direct stimulation of cancer cells with these compounds had no effect on their growth (Figure 7F). However, to assess the role of these compounds in terms of reducing tumor progression, we established a co-culture model. B16-F10 cells were seeded in removable inserts on the top of the plate and incubated with peritoneal macrophages from C57BL/6 mice seeded on the bottom of the plate and activated by LPS and treated with compounds or vehicle and then with ATP as an inflammasome activator. The cells were separated by a porous membrane that allowed free exchange of soluble factors and cytokines. Co-culture with activated macrophages treated with vehicle showed a larger tumor cell growth compared to that obtained with macrophages treated with our compounds (Figure 7G).

Thus, these compounds, in addition to reducing NLRP3-mediated inflammation and the release of proinflammatory cytokines, could reduce the activation of inflammation in the tumor microenvironment, which is responsible for accelerated tumor growth.

**In Vitro Metabolic Stability Studies.** Compounds **6c**, **7n**, and **10** were assessed for their metabolic stability to phase I oxidative metabolism using mouse and human liver microsomes, with 7-ethoxycoumarin (7-EC) and propranolol as control compounds, and results are shown in Table 2. The classification of the *in vitro* metabolic stability is reported in Table S1 (Supporting Information). Compounds **6c**, **7n**, and **10** showed a moderate intrinsic clearance after incubation with human liver microsomes. Compounds **7n** and **10** were metabolically unstable in the presence of the mouse liver microsomes, while compound **6c** was moderately stable in this species showing an intrinsic clearance of 4.8 $\mu$L/min/mg protein. Thus, compound **6c** was chosen for further pharmacokinetic characterization *in vivo*.

**Pharmacokinetic Characterization of Compound 6c *In Vivo*.** The preliminary PK profile of compound **6c** was evaluated in C57BL/6 mice. After IP injection at a dose of 25 mg/kg, compound **6c** was rapidly absorbed showing a $C_{max}$ of 1673 ± 333 ng/mL at the first sampling timepoint ($T_{max}$ = 5 min). After a rapid distribution phase, compound **6c** showed a quite long elimination phase with a favorable half-life of about 9 h. After 24 h, compound **6c** was well above the lowest limit of quantification (LLOQ) with a plasma concentration of 67 ± 6.5 ng/mL. A summary of the most relevant pharmacokinetic parameters in the female mice after intraperitoneal injection of 25 mg/kg of **6c** is given in Table 3.

## DISCUSSION AND CONCLUSIONS

Alterations in NLRP3 inflammasome activation have been associated with the pathogenesis of multiple diseases, including atherosclerosis, neurodegenerative diseases (Alzheimer's and Parkinson's), hereditary cryopyrin-associated periodic syndromes (CAPSs), metabolic diseases and cancer.[4,28] Therefore, it is not surprising that strategies targeting the NLRP3 inflammasome are hot topics of research and highlight its therapeutic promise as a molecular target. Few biopharmaceuticals, including the monoclonal antibody canakinumab (neutralizing IL-1$\beta$) and the recombinant protein anakinra (IL-1 receptor antagonist), are currently being used in the treatment of NLRP3-involving immunopathologies.[3] With respect to these "indirect" therapeutic strategies, the direct targeting of NLRP3


https://doi.org/10.1021/acs.jmedchem.3c00175
J. Med. Chem. XXXX, XXX, XXX−XXX

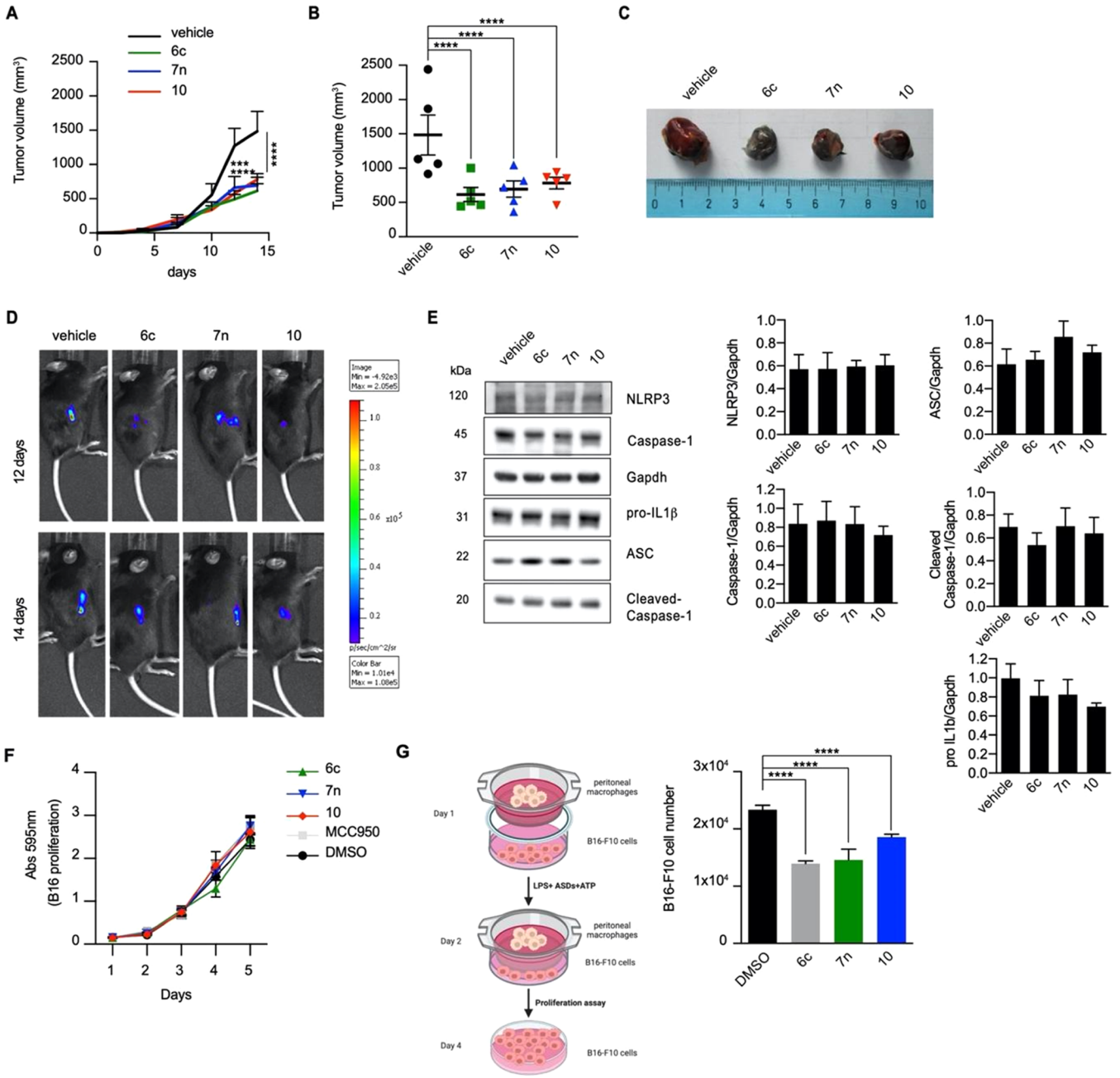


**Figure 7.** ASDs reduce cancer development. (A) C57BL/6 mice (5 for each condition) were subcutaneously inoculated with B16-F10cytLUC melanoma cells ($1 \times 10^6$). Tumor growth kinetics for the indicated time points. (B) *Ex vivo* quantification of tumor volumes assessed by a caliper. (C) Representative excised tumors imaged 14 days post-injection. (D) Representative pictures of cytLUC luminescence emission. (E) Representative western blot showing the amount of NLRP3, caspase-1, and ASC proteins levels in tumors from B16-F10cytLUC melanoma cells inoculated in C57BL/6 mice. Analysis for western blot was presented as the fold ratio over $\beta$-actin control (n = 5). No significant differences between tumors treated with vehicle or compounds. (F) Growth curve of B16-F10 cells after treatment with compounds. (G) Left, schematic representation of the co-culture assay (created with Biorender.com); right, peritoneal macrophages and B16-F10 cells were cultured in Transwell chambers and treated with LPS (1 $\mu$g/mL) for 2 h, then DMSO or compounds (1 $\mu$M) for 30 min, and finally stimulated with ATP for 1 h. After 48 h, B16-F10 cells were removed and counted. Error bars indicate s.e.m. $^{**}p < 0.01$, $^{****}p < 0.0001$.

by small molecules has the potential advantages of a more favorable cost/effectiveness ratio and possible oral administration. Moreover, the selective modulation of NLRP3 activity can be considered a less invasive approach than systemic IL-1 blockade, which may expose patients to the risk of infection. Also, the exclusive intervention of the IL-1/IL-1R signaling cascade may not be entirely effective in the treatment of NLRP3-driven diseases, in which more proinflammatory cytokines are likely to be involved, such as IL-18.

Various NLRP3 inflammasome inhibitors have been reported to interfere with inflammasome activation or inhibit downstream products of inflammasome activation that can affect cancer development.[3,4,29] In this study, we discovered a new series of potent and specific small-molecule inhibitors of NLRP3 that were obtained through a straightforward and low-cost


https://doi.org/10.1021/acs.jmedchem.3c00175
J. Med. Chem. XXXX, XXX, XXX−XXX

Table 2. In Vitro Determination of the Metabolic Stability after Incubation with Mouse and Human Liver Microsomes[a]

| | human liver microsomes (HLM) | | mouse liver microsomes (MLM) | |
|---|---|---|---|---|
| | mL/min/mg protein | min | mL/min/mg protein | min |
| compd | Cli ± SD | $t_{1/2}$ ± SD | Cli ± SD | $t_{1/2}$ ± SD |
| **6c** | 45.8 ± 6.0 | 30.5 ± 4.0 | 4.8 ± 0.5 | 287.8 ± 30.0 |
| **7n** | 28.7 ± 1.1 | 48.3 ± 1.8 | 270.2 ± 11.3 | 5.1 ± 0.2 |
| **10** | 31.9 ± 11.2 | 46.2 ± 16.2 | 123.5 ± 10.6 | 11.2 ± 1.0 |
| **7-EC**[b] | 168.2 ± 12.7 | 8.3 ± 0.6 | 422.2 ± 67.4 | 3.3 ± 0.5 |
| **Pro.**[c] | 30.6 ± 8.1 | 47.0 ± 12.4 | 198.1 ± 3.4 | 7.3 ± 0.1 |

[a]Results are expressed as mean ± SD, $n$ = 2. [b]7-EC, ethoxycoumarin. [c]Pro., propranolol. The standard compounds 7-EC and Prop. showed metabolic stability in agreement with the literature and internal validation data.

Table 3. Female Mouse Plasma Pharmacokinetic Parameters of Compound 6c (25 mg/kg, Intraperitoneal Injection)

| PK parameters | compound **6c** (25 mg/kg, IP) |
|---|---|
| $T_{1/2}$ | (h) 9.5 |
| $C_{max}$ (ng/mL) | 1.673 ± 333 |
| $T_{last}$ (h) | 24 |
| $C_{last\_obs}$ (ng/mL) | 67 ± 6.5 |
| (ng/mL*h) | 3.878 |

synthetic approach starting from commercially available proteinogenic and nonproteinogenic amino acids. Among the synthesized molecules, **6c**, **7n**, and **10** showed the most potent inhibitory activity *in vitro* ($IC_{50}$ values in the low nanomolar range) against NLRP3 inflammasome activation and subsequent IL-1$\beta$ release. Our combined SAR-molecular docking investigation allowed us to obtain the first insights into the structural requirements for the interaction of the newly discovered ASDs with NLRP3. The achieved results suggest a pharmacophoric model in which the central $\alpha/\beta$-amino acid residue of ASDs seems to have the main function of ensuring the proper distance and/or spatial orientation to the distal indacenamine and phenyl sulfonamide portions. This hypothesis was supported by the experimental evidence that the interposition of a $\beta$ alanine (**6**–**7k**) residue recovered the activity with respect to a glycine residue (see **6**–**7a**). In this case, given the absence of the amino acid side chain, the activity seems to be exclusively dependent on the proper distance between the distal portions of the molecule. However, the SAR analysis suggests that the spacing residue contributes to reinforcing the binding to the target protein since the inhibitory potency was significantly affected by the size and/or lipophilicity of the amino acid side chain and by the presence of polar functional groups. This phenomenon is evident in the case of the tyrosine derivative **10**, for which the docking analysis indicated an engagement of the phenolic hydroxyl group in the binding pocket of the putative target protein through hydrogen bonding. Additionally, the introduction of bulky and lipophilic side chains led to a marked enhancement of activity (such as in the case of **6c**) that has been ascribed to conformational effects together with the ability of the ligand to establish further hydrophobic contacts with NLRP3. The hypothesis that linker-related conformational factors particularly affect the activity of the identified molecules is even more evident when considering that the most active compound of the series is characterized by the presence of a cyclic amino acid residue (isoquinoline derivative **7n**). Collectively, the acquired structural information will be extremely useful for guiding possible future SAR optimization studies.

Of note, our compounds treatment had no effect on AIM2 or NLRC4 inflammasome, indicating their selectivity for the NLRP3 inflammasome. Furthermore, *in vivo* experiments revealed that these compounds attenuate LPS-induced inflammation, reducing IL-1$\beta$ release from blood and peritoneal exudates. Finally, we demonstrated that compounds **6c**, **7n**, and **10** significantly reduced tumor growth, reducing the activation of inflammation in the tumor microenvironment.

Despite the poor in vitro metabolic stability of compounds **7n** and **10** in the mouse species with respect to compound **6c**, all of the three reference compounds had shown significant pharmacological activity in vitro and in vivo. However, compound **6c** emerged as a compound suitable for proof-of-concept studies in the mouse in view of its favorable plasma exposure detected *in vivo* after intraperitoneal administration.

Thus, our preclinical research provides promising lead compounds that could be considered in further medicinal chemistry and pharmacological studies aimed at developing a new therapeutic approach for NLRP3 inflammasome-driven cancer.

## EXPERIMENTAL SECTION

**Chemistry.** *Materials and Methods.* Reagents and solvents were supplied by BLD, Sigma-Aldrich, and Fluorochem. Reaction progress was monitored by thin-layer chromatography (TLC) on precoated $F_{254}$ Macherey-Nagel plates of silica gel (UV lamp at 254 nm) and/or by electrospray mass spectrometer ESI MICROMASS ZMD 2000. Compounds were purified by crystallization or via semipreparative reverse-phase HPLC using a Waters 600 Multisolvent Delivery System, equipped with a Jupiter column C18 (250 × 30 mm$^2$, 300 Å, 15 $\mu$m spherical particle size) and a UV detector set on a wavelength of 220 nm. The column was perfused with a gradient, programmed time by time, of solution A (100% $H_2O$ and 0.1% v/v TFA) and solution B (40% $H_2O$, 60% $CH_3CN$, and 0.1%v/v TFA) at a flow rate of 20 mL/min. Analytical HPLC analyses were performed on a Beckman 116 liquid chromatograph equipped with a Beckman 166 diode array detector. Analytical purity of the final compounds was assessed using a Phenomenex Kinetex C18 column (150 × 4.6 mm, 5 $\mu$m particle size) and a variable wavelength UV detector set at 220 nm. All final compounds are >95% pure by HPLC analysis (see the Supporting Information). Analyses were conducted with an eluent consisting of $H_2O$ and $CH_3CN$, both containing 0.1% v/v TFA, at a flow rate of 0.5 mL/min, using a gradient from 0 to 100% of $CH_3CN$ over 25 min. $^1$H NMR and $^{13}$C NMR spectra were performed on a Varian 400 MHz spectrometer. The signals were referenced to residual $^1$H shift of the deuterated solvents (respectively, $\delta$ H 7.26 for $CDCl_3$; $\delta$ H 2.50 for DMSO-$d_6$). Chemical shifts ($\delta$) are expressed in parts per million (ppm), using the peak of tetramethylsilane as an internal standard in deuterated solvents, while values of coupling constants ($J$) are reported in Hertz (Hz). Splitting patterns are designed as s, singlet; d, doublet; t, triplet; q, quartet; m, multiplet; and b, broad. Infrared spectra were obtained in ATR mode using an FT-IR spectrometer (PerkinElmer Spectrum 100 FT-IR Spectrometer) between 4000 and 400 cm$^{-1}$. High-resolution mass was detected by an UltiMate 3000 UHPLC (Thermo Fisher) coupled to an Orbitrap Q-Exactive HRMS (see the


https://doi.org/10.1021/acs.jmedchem.3c00175
J. Med. Chem. XXXX, XXX, XXX−XXX

Supporting Information for further details). Melting points were determined using glass capillaries on a Stuart Scientific electrothermal apparatus SMP3 and are uncorrected.

*General Procedure for the Synthesis of* ***5a−n***. Sodium hydrogen carbonate ($NaHCO_3$, 2.5 mmol) was added to a solution of the amino acids **4a−n** (1.0 mmol) in water (5 mL) under vigorous stirring until all of the solutes had dissolved. Then, 4-nitrobenzenesulfonyl chloride (1.0 mmol) was added in small portions over 1 h and the reaction was stirred at room temperature for 16 h. Upon completion, the reaction mixture was acidified to pH 2 using 1 M HCl and the aqueous phase was extracted with ethyl acetate (3 × 15 mL). The combined organic layers were washed with brine (1 × 10 mL), dried over $Na_2SO_4$, and evaporated under reduced pressure. The residual crudes were crystallized to yield the desired products **5a−n**.

*((4-Nitrophenyl)sulfonyl)glycine (**5a**)*. White solid, crystallized from ethyl acetate/petroleum ether (60% yield). $^1$H NMR (400 MHz, DMSO-$d_6$): $\delta$ 12.66 (bs, 1H), 8.46 (t, $J$ = 6.1 Hz, 1H), 8.40−8.34 (m, 2H), 8.06−7.99 (m, 2H), 3.68 (d, $J$ = 6.1 Hz, 2H). MS (ESI): $m/z$ calcd for $C_8H_7N_2O_6S$ $[M - H]^-$ 259.21; found, 259.37.

*((4-Nitrophenyl)sulfonyl)-L-alanine (**5b**)*. White solid, crystallized from diethyl ether/petroleum ether (82% yield). $^1$H NMR (400 MHz, DMSO-$d_6$): $\delta$ 12.68 (s, 1H), 8.55 (s, 1H), 8.40−8.34 (m, 2H), 8.05−7.99 (m, 2H), 3.89−3.83 (m, 1H), 1.18 (d, $J$ = 7.2 Hz, 3H). MS (ESI): $m/z$ calcd for $C_9H_9N_2O_6S$ $[M - H]^-$ 273.24; found, 273.41.

*((4-Nitrophenyl)sulfonyl)-L-valine (**5c**)*. Yellowish solid, crystallized from diethyl ether/petroleum ether (60% yield). $^1$H NMR (400 MHz, DMSO-$d_6$): $\delta$ 12.63 (bs, 1H), 8.43 (d, $J$ = 9.5 Hz, 1H), 8.41−8.34 (m, 2H), 8.06−7.99 (m, 2H), 3.59 (dd, $J$ = 9.5, 5.9 Hz, 1H), 2.02−1.90 (m, 1H), 0.80 (dd, $J$ = 14.0, 6.8 Hz, 6H). MS (ESI): $m/z$ calcd for $C_{11}H_{13}N_2O_6S$ $[M - H]^-$ 301.29; found, 301.46.

*((4-Nitrophenyl)sulfonyl)-D-valine (**5d**)*. White solid, crystallized from diethyl ether/petroleum ether (52% yield). $^1$H NMR (400 MHz, DMSO-$d_6$): $\delta$ 12.63 (bs, 1H), 8.45 (d, $J$ = 9.5 Hz, 1H), 8.41 − 8.36 (m, 2H), 8.05 − 8.00 (m, 2H), 3.61 (dd, $J$ = 9.5, 5.9 Hz, 1H), 2.05 − 1.92 (m, 1H), 0.82 (dd, $J$ = 13.9, 6.8 Hz, 6H). MS (ESI): $m/z$ calcd for $C_{11}H_{13}N_2O_6S$ $[M - H]^-$ 301.29; found, 301.39.

*((4-Nitrophenyl)sulfonyl)-L-leucine (**5e**)*. Pale yellow solid, crystallized from ethyl acetate/petroleum ether (81% yield). $^1$H NMR (400 MHz, DMSO-$d_6$): $\delta$ 12.60 (bs, 1H), 8.57 (d, $J$ = 9.0 Hz, 1H), 8.42−8.37 (m, 2H), 8.04−8.00 (m, 2H), 3.78−3.72 (m, 1H), 1.63−1.54 (m, 1H), 1.45−1.40 (m, 2H), 0.84 (d, $J$ = 6.6 Hz, 3H), 0.75 (d, $J$ = 6.5 Hz, 3H). MS (ESI): $m/z$ calcd for $C_{12}H_{15}N_2O_6S$ $[M - H]^-$ 315.32; found, 315.48.

*(S)-2-((4-Nitrophenyl)sulfonamido)-2-phenylacetic Acid (**5f**)*. Off-white solid, crystallized from ethyl acetate/petroleum ether (74% yield). $^1$H NMR (400 MHz, DMSO-$d_6$): $\delta$ 13.03 (bs, 1H), 9.11 (d, $J$ = 9.3 Hz, 1H), 8.29−8.21 (m, 2H), 7.96−7.89 (m, 2H), 7.26−7.18 (m, 5H), 4.98 (d, $J$ = 9.0 Hz, 1H). MS (ESI): $m/z$ calcd for $C_{14}H_{11}N_2O_6S$ $[M - H]^-$ 335.31; found, 335.45.

*((4-Nitrophenyl)sulfonyl)-L-phenylalanine (**5g**)*. Off-white solid, crystallized from ethyl acetate/petroleum ether (81% yield). $^1$H NMR (400 MHz, DMSO-$d_6$): $\delta$ 12.85 (bs, 1H), 8.70 (d, $J$ = 8.5 Hz, 1H), 8.22−8.14 (m, 2H), 7.77−7.67 (m, 2H), 7.15−7.03 (m, 5H), 3.94 (t, $J$ = 10.0 Hz, 1H), 2.99−2.95 (m, 1H), 2.72−2.70 (m, 1H). MS (ESI): $m/z$ calcd for $C_{15}H_{13}N_2O_6S$ $[M - H]^-$ 349,34; found, 349.51.

*((4-Nitrophenyl)sulfonyl)-D-phenylalanine (**5h**)*. Off-white solid, crystallized from ethyl acetate/petroleum ether (78% yield). $^1$H NMR (400 MHz, DMSO-$d_6$): $\delta$ 12.82 (bs, 1H), 8.64 (d, $J$ = 8.5 Hz, 1H), 8.20−8.11 (m, 2H), 7.75−7.67 (m, 2H), 7.18−7.05 (m, 5H), 3.97−3.89 (m, 1H), 2.99−2.95 (m, 1H), 2.72−2.70 (m, 1H). MS (ESI): $m/z$ calcd for $C_{15}H_{13}N_2O_6S$ $[M - H]^-$ 349,34; found, 349.53.

*(S)-3-(4-(tert-Butoxy)phenyl)-2-((4-nitrophenyl)sulfonamido)-propanoic Acid (**5i**)*. Brownish solid, crystallized from diethyl ether/methanol (71% yield). $^1$H NMR (400 MHz, DMSO-$d_6$): 12.84 (bs, 1H), 8.70 (d, $J$ = 9.1 Hz, 1H), 8.26−8.17 (m, 2H), 7.77−7.73 (m, 2H), 7.05−6.95 (m, 2H), 6.73−6.63 (m, 2H), 3.96−3.90 (m, 1H), 2.94 (dd, $J$ = 13.8, 4.7 Hz, 1H), 2.68−2.65 (m, 1H), 1.21 (s, 9H). MS (ESI): $m/z$ calcd for $C_{19}H_{21}N_2O_7S$ $[M - H]^-$ 421.44; found, 421.29.

*$N^6$-(tert-Butoxycarbonyl)-$N^2$-((4-nitrophenyl)sulfonyl)-L-lysine (**5j**)*. Pale yellow solid, crystallized from ethyl acetate/petroleum ether (80% yield). $^1$H NMR (400 MHz, DMSO-$d_6$): $\delta$ 12.62 (bs, 1H), 8.52 (d, $J$ = 8.8 Hz, 1H), 8.42−8.33 (m, 2H), 8.04−7.96 (m, 2H), 6.70 (t, $J$ = 5.5 Hz, 1H), 3.73−3.68 (m, 1H), 2.80−2.75 (m, 2H), 1.65−1.41 (m, 2H), 1.34 (s, 9H), 1.26−1.22 (m, 4H). MS (ESI): $m/z$ calcd for $C_{17}H_{26}N_3O_8S$ $[M + H]^+$ 432.47; found, 432.20, 376.23 $[M - tBu]^+$, 332.18 $[M - Boc]^+$.

*3-((4-Nitrophenyl)sulfonamido)propanoic Acid (**5k**)*. Off-white solid, crystallized from diethyl ether/petroleum ether (69% yield). $^1$H NMR (400 MHz, DMSO-$d_6$): $\delta$ 12.26 (s, 1H), 8.43−8.37 (m, 2H), 8.07 (bs, 1H), 8.05−8.00 (m, 2H), 3.00−2.97 (m, 2H), 2.36 (t, $J$ = 6.9 Hz, 2H). MS (ESI): $m/z$ calcd for $C_9H_9N_2O_6S$ $[M - H]^-$ 273.24; found, 273.45.

*((4-Nitrophenyl)sulfonyl)proline (**5l**)*. Pale yellow solid, crystallized from ethyl acetate/petroleum ether (65% yield). $^1$H NMR (400 MHz, DMSO-$d_6$): $\delta$ 12.84 (bs, 1H), 8.42−8.36 (m, 2H), 8.11−8.06 (m, 2H), 4.20 (dd, $J$ = 8.6, 3.8 Hz, 1H), 3.44−3.35 (m, 1H), 3.25−3.21 (m, 1H), 2.02−1.94 (m, 1H), 1.91−1.75 (m, 2H), 1.71−1.60 (m, 1H). MS (ESI): $m/z$ calcd for $C_{11}H_{11}N_2O_6S$ $[M - H]^-$ 299.28; found, 299.81.

*1-((4-Nitrophenyl)sulfonyl)piperidine-2-carboxylic Acid (**5m**)*. Pale yellow solid, crystallized from ethyl acetate/petroleum ether (55% yield). $^1$H NMR (400 MHz, DMSO-$d_6$): $\delta$ 12.97 (bs, 1H), 8.42−8.33 (m, 2H), 8.08−8.00 (m, 2H), 4.62 (d, $J$ = 5.2 Hz, 1H), 3.75−3.71 (m, 1H), 3.20−3.09 (m, 1H), 2.07−2.00 (m, 1H), 1.62−1.58 (m, 3H), 1.30−1.18 (m, 2H). MS (ESI): $m/z$ calcd for $C_{12}H_{13}N_2O_6S$ $[M - H]^-$ 313.30; found, 313.36.

*(S)-2-((4-Nitrophenyl)sulfonyl)-1,2,3,4-tetrahydroisoquinoline-3-carboxylic Acid (**5n**)*. Foamy yellow solid, crystallized from diethyl ether/methanol (48% yield). $^1$H NMR (400 MHz, DMSO-$d_6$): $\delta$ 12.97 (bs, 1H), 8.40−8.33 (m, 2H), 8.16−8.09 (m,2H), 7.15 (q, $J$ = 3.6 Hz, 4H), 4.93 (dd, $J$ = 6.2, 3.2 Hz, 1H), 4.66 (d, $J$ = 15.8 Hz, 1H), 4.46 (d, $J$ = 15.8 Hz, 1H), 3.17−3.05 (m, 2H). MS (ESI): $m/z$ calcd for $C_{16}H_{13}N_2O_6S$ $[M - H]^-$ 361.35; found, 361.30.

*General Procedure for the Preparation of Compounds* ***6a−n*** *and* ***8−9***. HATU (1.1 mmol) and DIPEA (1.1 mmol) were added to an ice-cooled solution of the appropriate carboxylic acid **5a−n** (1.1 mmol) in DMF (5 mL). Then, a solution of hexahydro-s-indacen-4-amine (1.0 mmol) in DMF (2 mL) was added dropwise while maintaining the temperature at 0 °C. The resulting mixture was warmed to room temperature and left stirring until the reaction was complete. After the removal of the solvent, the crude was dissolved using ethyl acetate (20 mL) and the organic layer was sequentially washed with 10% aqueous solution of citric acid (1 × 10 mL), 5% aqueous solution of $NaHCO_3$ (1 × 10 mL), and brine (1 × 10 mL). After drying over $Na_2SO_4$, the solvent was evaporated to yield a solid residue which was first triturated with diethyl ether, then filtered, and the solid was recrystallized from methanol to give the derivatives **6a−n**. The intermediates **6i** and **6j** were, respectively, deprotected by treatment with 4N HCl in dioxane (7 mL) at room temperature. After completion of the reaction, the solvent was removed, and the crudes were purified via semipreparative HPLC to furnish the unprotected compounds **8** and **9**.

*N-(1,2,3,5,6,7-Hexahydro-s-indacen-4-yl)-2-((4-nitrophenyl)-sulfonamido)acetamide (**6a**)*. White solid (67% yield); mp 181−182 °C. $^1$H NMR (400 MHz, DMSO-$d_6$): $\delta$ 9.39 (s, 1H), 8.53 (s, 1H), 8.48−8.36 (m, 2H), 8.14−7.99 (m, 2H), 6.91 (s, 1H), 3.79 (s, 2H), 2.77 (t, $J$ = 7.4 Hz, 4H), 2.49−2.43 (m, 4H), 1.93−1.85 (m, 4H). $^{13}$C NMR (DMSO-$d_6$): $\delta$ 165.12, 149.32, 146.25, 142.71, 137.07, 128.94, 128.20, 124.25, 117.81, 44.78, 32.29, 30.11, 24.89. MS (ESI): $m/z$ calcd for $C_{20}H_{22}N_3O_5S$ $[M + H]^+$ 416.47; found, 416.33. $T_R$ = 18,98 min.

*(S)-N-(1,2,3,5,6,7-Hexahydro-s-indacen-4-yl)-2-((4-nitrophenyl)-sulfonamido)propanamide (**6b**)*. White solid (77% yield); mp 298−300 °C. $^1$H NMR (400 MHz, DMSO-$d_6$): $\delta$ 9.48 (s, 1H), 8.68 (d, $J$ = 7.5 Hz, 1H), 8.41 (d, $J$ = 8.7 Hz, 2H), 8.09 (d, $J$ = 8.8 Hz, 2H), 6.91 (s, 1H), 4.18−4.07 (m, 1H), 2.76 (t, $J$ = 7.4 Hz, 4H), 2.40 (t, $J$ = 7.4 Hz, 4H), 1.88−1.84 (m, 4H), 1.30 (d, $J$ = 6.7 Hz, 3H). $^{13}$C NMR (DMSO-$d_6$): $\delta$ 169.51, 149.82, 147.42, 143.24, 137.71, 129.40, 128.63, 124.83, 118.41, 52.33, 32.82, 30.46, 25.39, 20.63. MS (ESI): $m/z$ calcd for $C_{21}H_{24}N_3O_5S$ $[M + H]^+$ 430.50; found, 430.35. $T_R$ = 20,77 min.

*(S)-N-(1,2,3,5,6,7-Hexahydro-s-indacen-4-yl)-3-methyl-2-((4-nitrophenyl)sulfonamido)butanamide (**6c**)*. White solid (79% yield); mp 250−252 °C. $^1$H NMR (400 MHz, DMSO-$d_6$): $\delta$ 9.38 (s, 1H), 8.45


https://doi.org/10.1021/acs.jmedchem.3c00175
J. Med. Chem. XXXX, XXX, XXX−XXX

(bs, 1H), 8.37 (d, $J$ = 8.9 Hz, 2H), 8.05 (d, $J$ = 8.9 Hz, 2H), 6.87 (s, 1H), 3.80 (d, $J$ = 6.2 Hz, 1H), 2.74−2.70 (m, 4H), 2.38−2.19 (m, 4H), 1.98 (dq, $J$ = 13.4, 6.6 Hz, 1H), 1.89−1.73 (m, 4H), 0.93 (d, $J$ = 6.7 Hz, 3H), 0.85 (d, $J$ = 6.8 Hz, 3H). $^{13}$C NMR (DMSO-$d_6$): δ 149.58, 143.23, 137.53, 129.46, 128.56, 124.72, 118.35, 62.16, 32.80, 31.86, 30.63, 25.35, 19.79, 18.25. MS (ESI): $m/z$ calcd for $C_{23}H_{28}N_3O_5S$ $[M + H]^+$ 458.55; found, 458.28. $T_R$ = 21,00 min.

*(R)-N-(1,2,3,5,6,7-Hexahydro-s-indacen-4-yl)-3-methyl-2-((4-nitrophenyl)sulfonamido)butanamide* ***(6d)***. White solid (88% yield); mp 300−302 °C. $^1$H NMR (400 MHz, DMSO-$d_6$): δ 9.51 (s, 1H), 8.49 (d, $J$ = 7.5 Hz, 1H), 8.43−8.31 (m, 2H), 8.13−8.01 (m, 2H), 6.87 (s, 1H), 3.85 (t, $J$ = 6.7 Hz, 1H), 2.71 (t, $J$ = 7.3 Hz, 4H), 2.37−2.17 (m, 4H), 2.05−1.93 (m, 1H), 1.86−1.72 (m, 4H), 0.95 (d, $J$ = 6.7 Hz, 3H), 0.86 (d, $J$ = 6.8 Hz, 3H). $^{13}$C NMR (DMSO-$d_6$): δ 168.18, 149.73, 147.66, 143.20, 137.61, 129.44, 128.68, 124.77, 118.37, 62.05, 32.79, 31.81, 30.63, 25.33, 19.74, 18.30. MS (ESI): $m/z$ calcd for $C_{23}H_{28}N_3O_5S$ $[M + H]^+$ 458.55; found, 457.70. $T_R$ = 21,88 min.

*(S)-N-(1,2,3,5,6,7-Hexahydro-s-indacen-4-yl)-4-methyl-2-((4-nitrophenyl)sulfonamido)pentanamide* ***(6e)***. White solid (78% yield); mp 291−293 °C. $^1$H NMR (400 MHz, DMSO-$d_6$): δ 9.47 (s, 1H), 8.60 (s, 1H), 8.44−8.35 (m, 2H), 8.09−8.01 (m, 2H), 6.88 (s, 1H), 4.05−4.01 (m, 1H), 2.73 (t, $J$ = 7.3 Hz, 4H), 2.32 (t, $J$ = 7.4 Hz, 4H), 1.93−1.77 (m, 4H), 1.72−1.64 (m, 1H), 1.55−1.38 (m, 2H), 0.89 (d, $J$ = 6.7 Hz, 3H), 0.83 (d, $J$ = 6.6 Hz, 3H). $^{13}$C NMR (DMSO-$d_6$): δ 169.30, 149.75, 147.61, 143.22, 137.70, 129.40, 128.62, 124.78, 118.41, 55.19, 42.81, 32.81, 30.47, 25.40, 24.49, 23.34, 21.75. MS (ESI): $m/z$ calcd for $C_{24}H_{30}N_3O_5S$ $[M + H]^+$ 472.58; found, 472.52. $T_R$ = 25.77 min.

*(S)-N-(1,2,3,5,6,7-Hexahydro-s-indacen-4-yl)-2-((4-nitrophenyl)-sulfonamido)-2-phenylacetamide* ***(6f)***. White solid (69% yield); mp 235−237 °C. $^1$H NMR (400 MHz, DMSO-$d_6$): δ 9.69 (s, 1H), 9.22 (d, $J$ = 9.2 Hz, 1H), 8.32 (d, $J$ = 8.8 Hz, 2H), 8.02 (d, $J$ = 8.7 Hz, 2H), 7.42 (d, $J$ = 6.9 Hz, 2H), 7.30−7.22 (m, 3H), 6.89 (s, 1H), 5.30 (d, $J$ = 9.2 Hz, 1H), 2.72 (t, $J$ = 7.2 Hz, 4H), 2.36−2.12 (m, 4H), 1.91−1.66 (m, 4H). $^{13}$C NMR (DMSO-$d_6$): δ 166.43, 149.10, 146.72, 142.75, 137.30, 137.00, 128.53, 128.10, 127.69, 126.90, 124.04, 117.96, 59.39, 32.16, 29.72, 24.79. MS (ESI): $m/z$ calcd for $C_{26}H_{26}N_3O_5S$ $[M + H]^+$ 492.57; found, 492.50. $T_R$ = 21,98 min.

*(S)-N-(1,2,3,5,6,7-Hexahydro-s-indacen-4-yl)-2-((4-nitrophenyl)-sulfonamido)-3-phenylpropanamide* ***(6g)***. White solid (84% yield); mp 196−197 °C. $^1$H NMR (400 MHz, DMSO-$d_6$): δ 9.54 (s, 1H), 8.82−8.79 (m, 1H), 8.26 (d, $J$ = 8.5 Hz, 2H), 7.86 (d, $J$ = 8.7 Hz, 2H), 7.21−7.16 (m, 5H), 6.91 (s, 1H), 4.31−4.27 (m, 1H), 3.44−3.37 (m, 1H), 3.00−2.97 (m, 1H), 2.81−2.74 (m, 4H), 2.41−2.27 (m, 4H), 1.88−1.83 (m, 4H). $^{13}$C NMR (DMSO-$d_6$): δ 168.62, 149.55, 147.48, 143.25, 137.66, 137.29, 129.82, 129.30, 128.49, 128.24, 126.81, 124.64, 118.41, 58.18, 32.83, 30.47, 25.46. MS (ESI): $m/z$ calcd for $C_{27}H_{28}N_3O_5S$ $[M + H]^+$ 506.60; found, 506.50. $T_R$ = 22,43 min.

*(R)-N-(1,2,3,5,6,7-Hexahydro-s-indacen-4-yl)-2-((4-nitrophenyl)-sulfonamido)-3-phenylpropanamide* ***(6h)***. White solid (73% yield); mp 201−203 °C. $^1$H NMR (400 MHz, DMSO-$d_6$): δ 9.54 (s, 1H), 8.80 (bs, 1H), 8.26 (d, $J$ = 8.6 Hz, 2H), 7.86 (d, $J$ = 8.4 Hz, 2H), 7.21−7.17 (m, 5H), 6.91 (s, 1H), 4.32−4.26 (m, 1H), 3.02−2.97 (m, 1H), 2.81−2.74 (m, 5H), 2.42−2.28 (m, 4H), 2.01−1.72 (m, 4H). $^{13}$C NMR (DMSO-$d_6$): δ 168.61, 149.55, 147.48, 143.24, 137.66, 129.82, 128.24, 126.81, 124.64, 118.41, 58.18, 32.83, 30.47, 25.46. MS (ESI): $m/z$ calcd for $C_{27}H_{28}N_3O_5S$ $[M + H]^+$ 506.60; found, 506.45. $T_R$ = 23,29 min.

*(S)-3-(4-(tert-Butoxy)phenyl)-N-(1,2,3,5,6,7-hexahydro-s-indacen-4-yl)-2-((4-nitrophenyl)sulfonamido)propanamide* ***(6i)***. White solid (79% yield). $^1$H NMR (400 MHz, DMSO-$d_6$): δ 9.55 (s, 1H), 8.83−8.79 (m, 1H), 8.33−8.25 (m, 2H), 7.94−7.85 (m, 2H), 7.14−7.06 (m, 2H), 6.91 (s, 1H), 6.81−6.73 (m, 2H), 4.29−4.22 (m, 1H), 2.76 (t, $J$ = 7.3 Hz, 6H), 2.42−2.29 (m, 4H), 1.91−1.78 (m, 5H), 1.24 (s, 9H). $^{13}$C NMR (DMSO-$d_6$): δ 168.09, 153.55, 148.97, 147.05, 142.66, 137.10, 131.15, 129.72, 128.77, 127.67, 127.08, 124.11, 123.01, 117.82, 77.39, 57.75, 38.22, 32.25, 29.92, 28.32, 24.90. MS (ESI): $m/z$ calcd for $C_{31}H_{36}N_3O_6S$ $[M + H]^+$ 578.70; found, 578.55.

*(S)-N-(1,2,3,5,6,7-Hexahydro-s-indacen-4-yl)-3-(4-hydroxyphenyl)-2-((4-nitrophenyl)sulfonamido)propanamide* ***(8)***. Pale yellow solid (71% yield); mp 200−202 °C. $^1$H NMR (400 MHz, DMSO-$d_6$): δ 9.52 (s, 1H), 8.71 (d, $J$ = 9.1 Hz, 1H), 8.27−8.20 (m, 2H), 7.86−7.78 (m, 2H), 7.00−6.93 (m, 2H), 6.89 (s, 1H), 6.57−6.47 (m, 2H), 4.21−4.15 (m, 1H), 2.86 (dd, $J$ = 13.7, 5.3 Hz, 1H), 2.74 (t, $J$ = 7.3 Hz, 4H), 2.67−2.61 (m, 1H), 2.46−2.25 (m, 4H), 1.91−1.79 (m, 4H). $^{13}$C NMR (DMSO-$d_6$): δ 168.27, 155.98, 148.85, 147.02, 142.65, 137.11, 130.14, 128.83, 127.66, 126.69, 124.00, 117.79, 114.62, 58.11, 32.27, 29.94, 24.89. MS (ESI): $m/z$ calcd for $C_{27}H_{28}N_3O_6S$ $[M + H]^+$ 522.60; found 522.62. $T_R$ = 19,73 min.

*tert-Butyl (S)-(6-((1,2,3,5,6,7-hexahydro-s-indacen-4-yl)amino)-5-((4-nitrophenyl)sulfonamido)-6-oxohexyl)carbamate* ***(6j)***. White solid (83% yield). $^1$H NMR (400 MHz, DMSO-$d_6$): δ 9.45 (s, 1H), 8.60 (bs, 1H), 8.45−8.36 (m, 2H), 8.13−8.03 (m, 2H), 6.90 (s, 1H), 6.76 (t, $J$ = 5.8 Hz, 1H), 4.06−3.88 (m, 1H), 2.87−2.82 (m, 2H), 2.75 (t, $J$ = 7.3 Hz, 4H), 2.35 (t, $J$ = 7.1 Hz, 4H), 1.89−1.81 (m, 4H), 1.75−1.47 (m, 2H), 1.36 (s, 9H), 1.32−1.18 (m, 4H). $^{13}$C NMR (DMSO-$d_6$): δ 168.42, 155.40, 149.14, 142.66, 137.06, 128.85, 128.00, 124.21, 117.81, 77.20, 57.26, 56.08, 33.16, 32.23, 29.95, 28.82, 28.14, 24.82, 22.39. MS (ESI): $m/z$ calcd for $C_{29}H_{39}N_4O_7S$ $[M + H]^+$ 587.71; found, 587.58, 531.53 $[M - tBu]^+$, 487.57 $[M - Boc]^+$.

*(S)-6-Amino-N-(1,2,3,5,6,7-hexahydro-s-indacen-4-yl)-2-((4-nitrophenyl)sulfonamido)hexanamide* ***(9)***. White solid (70% yield); mp 225−227 °C. $^1$H NMR (400 MHz, DMSO-$d_6$): δ 9.64 (s, 1H), 8.66 (d, $J$ = 9.1 Hz, 1H), 8.43−8.36 (m, 2H), 8.13−8.05 (m, 2H), 7.95 (s, 3H), 6.90 (s, 1H), 4.08−4.03 (m, 1H), 2.74 (t, $J$ = 7.4 Hz, 6H), 2.34 (t, $J$ = 7.4 Hz, 4H), 1.90−1.77 (m, 4H), 1.75−1.68 (m, 1H), 1.66−1.51 (m, 3H), 1.39−1.29 (m, 2H). $^{13}$C NMR (DMSO-$d_6$): δ 168.88, 149.85, 147.52, 143.28, 137.72, 129.45, 128.75, 124.89, 118.46, 56.54, 38.91, 33.43, 32.87, 30.62, 26.77, 25.44, 22.66. MS (ESI): $m/z$ calcd for $C_{24}H_{31}N_4O_5S$ $[M + H]^+$ 487.59; found, 487.59. $T_R$ = 17,67 min.

*N-(1,2,3,5,6,7-Hexahydro-s-indacen-4-yl)-3-((4-nitrophenyl)-sulfonamido)propanamide* ***(6k)***. Off-white solid (89% yield); mp 224−226 °C. $^1$H NMR (400 MHz, DMSO-$d_6$): δ 9.36 (s, 1H), 8.43 (d, $J$ = 7.4 Hz, 2H), 8.11−8.06 (m, 3H), 6.93 (s, 1H), 3.12−3.06 (m, 2H), 2.79 (t, $J$ = 7.5 Hz, 4H), 2.62 (t, $J$ = 7.4 Hz, 4H), 2.48−2.43 (m, 2H), 1.96−1.92 (m, 4H). $^{13}$C NMR (DMSO-$d_6$): δ 167.92, 150.01, 146.44, 143.18, 137.77, 130.07, 128.56, 125.08, 118.20, 39.66, 36.05, 32.91, 30.80, 25.51. MS (ESI): $m/z$ calcd for $C_{21}H_{24}N_3O_5S$ $[M + H]^+$ 430.50; found, 430.43. $T_R$ = 20,70 min.

*N-(1,2,3,5,6,7-Hexahydro-s-indacen-4-yl)-1-((4-nitrophenyl)-sulfonyl)pyrrolidine-2-carboxamide* ***(6l)***. White solid (88% yield); mp 235−236 °C. $^1$H NMR (400 MHz, DMSO-$d_6$): δ 9.48 (s, 1H), 8.42 (d, $J$ = 8.9 Hz, 2H), 8.19−8.07 (m, 2H), 6.95 (s, 1H), 4.26−4.23 (m, 1H), 3.61−3.49 (m, 1H), 2.80 (t, $J$ = 7.3 Hz, 4H), 2.66 (t, $J$ = 7.4 Hz, 4H), 2.03−1.84 (m, 8H), 1.72−1.59 (m, 1H). $^{13}$C NMR (DMSO-$d_6$): δ 168.97, 149.82, 142.67, 137.61, 129.63, 129.03, 127.93, 125.40, 123.65, 118.74, 117.19, 62.16, 60.71, 32.35, 31.32, 29.97, 26.23, 24.94. MS (ESI): $m/z$ calcd for $C_{23}H_{26}N_3O_5S$ $[M + H]^+$ 456.54; found, 456.41. $T_R$ = 21,81 min.

*N-(1,2,3,5,6,7-Hexahydro-s-indacen-4-yl)-1-((4-nitrophenyl)-sulfonyl)piperidine-2-carboxamide* ***(6m)***. White solid (77% yield); mp 242−244 °C. $^1$H NMR (400 MHz, DMSO-$d_6$): δ 9.42 (s, 1H), 8.51−8.25 (m, 2H), 8.12−7.86 (m, 2H), 6.92 (s, 1H), 4.76−4.72 (m, 1H), 3.84−3.80 (m, 1H), 3.66−3.55 (m, 1H), 2.78 (t, $J$ = 7.3 Hz, 4H), 2.60−2.53 (m, 4H), 2.14−2.10 (m, 1H), 2.01−1.85 (m, 4H), 1.74−1.62 (m, 3H), 1.40−1.33 (m, 2H). $^{13}$C NMR (DMSO-$d_6$): δ 167.65, 149.36, 145.24, 142.73, 137.28, 128.87, 128.21, 124.30, 117.93, 54.40, 42.87, 32.27, 30.10, 28.85, 24.83, 24.24, 18.95. MS (ESI): $m/z$ calcd for $C_{24}H_{28}N_3O_5S$ $[M + H]^+$ 470.56; found, 470.24. $T_R$ = 21,27 min.

*(S)-N-(1,2,3,5,6,7-Hexahydro-s-indacen-4-yl)-2-((4-nitrophenyl)-sulfonyl)-1,2,3,4-tetrahydroisoquinoline-3-carboxamide* ***(6n)***. Pale yellow solid (84% yield); mp 156−158 °C. $^1$H NMR (400 MHz, DMSO-$d_6$): δ 9.47 (s, 1H), 8.39−8.31 (m, 2H), 8.16−8.08 (m, 2H), 7.21−7.12 (m, 4H), 6.90 (s, 1H), 4.79 (t, $J$ = 5.3 Hz, 1H), 4.74−4.60 (m, 2H), 3.13 (t, $J$ = 5.8 Hz, 2H), 2.75 (t, $J$ = 7.3 Hz, 4H), 2.47−2.34 (m, 4H), 1.90−1.83 (m, 4H). $^{13}$C NMR (DMSO-$d_6$): δ 167.51, 149.60, 143.64, 142.64, 137.39, 132.24, 131.65, 128.81, 128.65, 127.90, 126.76, 126.32, 125.97, 124.35, 117.89, 54.88, 45.35, 32.44, 32.25, 29.82, 24.82. MS (ESI): $m/z$ calcd for $C_{28}H_{28}N_3O_5S$ $[M + H]^+$ 518.61; found, 518.60. $T_R$ = 21,53 min.


https://doi.org/10.1021/acs.jmedchem.3c00175
J. Med. Chem. XXXX, XXX, XXX−XXX

*General Procedure for the Preparation of Compounds **7a−n** and **10−11**.* The nitro derivatives **6a−n** (1 mmol) were dissolved in ethyl acetate (15 mL) and glacial $CH_3COOH$ (0.5 mL). A catalytic amount (0.1 mmol) of palladium on activated charcoal (10% Pd basis) was added under hydrogen atmosphere. After 16 h, the reaction mixture was filtered through Celite, which was washed three times with methanol (3 × 20 mL). The solvent was concentrated under reduced pressure, and the crudes were purified via semipreparative HPLC to give compounds **7a−n**. For obtaining the final compounds **10** and **11**, **7i−j** were deprotected as described for **6i−j**.

*2-((4-Aminophenyl)sulfonamido)-N-(1,2,3,5,6,7-hexahydro-s-indacen-4-yl)acetamide (**7a**).* White solid (91% yield); mp 95−97 °C. $^1$H NMR (400 MHz, DMSO-$d_6$): $\delta$ 9.25 (s, 1H), 7.50−7.38 (m, 3H), 6.92 (s, 1H), 6.64−6.53 (m, 2H), 5.94 (bs, 2H), 3.51 (d, $J$ = 6.1 Hz, 2H), 2.77 (t, $J$ = 7.3 Hz, 4H), 2.57 (t, $J$ = 7.4 Hz, 4H), 1.99−1.87 (m, 4H). $^{13}$C NMR (DMSO-$d_6$): $\delta$ 165.71, 152.55, 142.69, 137.23, 129.12, 128.54, 124.82, 117.75, 112.48, 45.14, 32.35, 30.17, 25.01. MS (ESI): $m/z$ calcd for $C_{20}H_{24}N_3O_3S$ $[M + H]^+$ 386.49; found, 386.32. $T_R$ = 20,77 min.

*(S)-2-((4-Aminophenyl)sulfonamido)-N-(1,2,3,5,6,7-hexahydro-s-indacen-4-yl)propanamide (**7b**).* White solid (88% yield); mp 228−229 °C. $^1$H NMR (400 MHz, DMSO-$d_6$): $\delta$ 9.22 (s, 1H), 7.47 (d, $J$ = 8.1 Hz, 1H), 7.42 (d, $J$ = 8.7 Hz, 2H), 6.91 (s, 1H), 6.56 (d, $J$ = 8.7 Hz, 2H), 5.89 (s, 2H), 3.87−3.80 (m, 1H), 2.77 (t, $J$ = 7.2 Hz, 4H), 2.54−2.51 (m, 4H), 1.97−1.89 (m, 4H), 1.17 (dd, $J$ = 7.0, 4.0 Hz, 3H). $^{13}$C NMR (DMSO-$d_6$): $\delta$ 170.25, 152.98, 143.22, 137.82, 129.63, 128.90, 126.40, 118.28, 112.98, 52.18, 32.88, 30.54, 25.55, 20.37. MS (ESI): $m/z$ calcd for $C_{21}H_{26}N_3O_3S$ $[M + H]^+$ 400.52; found, 400.40. $T_R$ = 19,78 min.

*(S)-2-((4-Aminophenyl)sulfonamido)-N-(1,2,3,5,6,7-hexahydro-s-indacen-4-yl)-3-methylbutanamide (**7c**).* White solid (98% yield); mp 281−283 °C. $^1$H NMR (400 MHz, DMSO-$d_6$): $\delta$ 9.25 (s, 1H), 7.46−7.35 (m, 2H), 7.14 (d, $J$ = 8.3 Hz, 1H), 6.90 (s, 1H), 6.57−6.47 (m, 2H), 5.85 (s, 2H), 3.62 (t, $J$ = 7.1 Hz, 1H), 2.75 (t, $J$ = 7.4 Hz, 4H), 2.48−2.44 (m, 4H), 1.94−1.87 (m, 5H), 0.90 (d, $J$ = 6.7 Hz, 3H), 0.81 (d, $J$ = 6.8 Hz, 3H). $^{13}$C NMR (DMSO-$d_6$): $\delta$ 168.37, 152.36, 142.62, 137.20, 129.10, 128.35, 126.08, 117.67, 112.29, 61.01, 32.30, 31.22, 30.18, 24.98, 19.22, 17.57. MS (ESI): $m/z$ calcd for $C_{23}H_{30}N_3O_3S$ $[M + H]^+$ 428.57; found 428.29. $T_R$ = 19,43 min.

*(R)-2-((4-Aminophenyl)sulfonamido)-N-(1,2,3,5,6,7-hexahydro-s-indacen-4-yl)-3-methylbutanamide (**7d**).* White solid (87% yield); mp 284−286 °C. $^1$H NMR (400 MHz, DMSO-$d_6$): $\delta$ 9.25 (s, 1H), 7.45−7.32 (m, 2H), 7.13 (d, $J$ = 8.9 Hz, 2H), 6.90 (s, 1H), 6.59−6.47 (m, 2H), 3.64−.360 (m, 2H), 2.75 (t, $J$ = 7.3 Hz, 4H), 2.47−2.44 (m, 4H), 1.94−1.87 (m, 5H), 0.90 (d, $J$ = 6.7 Hz, 3H), 0.81 (d, $J$ = 6.8 Hz, 3H). $^{13}$C NMR (DMSO-$d_6$): $\delta$ 173.69, 157.59, 147.94, 142.52, 134.41, 133.67, 131.46, 123.00, 117.67, 66.33, 37.62, 36.54, 35.50, 30.30, 24.54, 22.88. MS (ESI): $m/z$ calcd for $C_{23}H_{30}N_3O_3S$ $[M + H]^+$ 428.16; found 428.53. $T_R$ = 24,87 min.

*(S)-2-((4-Aminophenyl)sulfonamido)-N-(1,2,3,5,6,7-hexahydro-s-indacen-4-yl)-4-methylpentanamide (**7e**).* White solid (73% yield); mp 188−190 °C. $^1$H NMR (400 MHz, DMSO-$d_6$): $\delta$ 9.30 (s, 1H), 7.48−7.38 (m, 3H), 6.92 (s, 1H), 6.60−6.50 (m, 2H), 3.82−3.76 (m, 1H), 2.78 (t, J = 7.4 Hz, 4H), 2.57−2.53 (m, 3H), 2.46−2.40 (m, 1H), 2.01−1.85 (m, 4H), 1.72−1.59 (m, 1H), 1.44−1.34 (m, 2H), 0.85 (d, J = 6.7 Hz, 3H), 0.76 (d, J = 6.5 Hz, 3H). $^{13}$C NMR (DMSO-$d_6$): $\delta$ 169.62, 152.32, 142.62, 137.32, 129.15, 128.34, 126.14, 117.68, 112.36, 54.55, 42.37, 32.33, 30.04, 25.03, 23.84, 22.83, 21.38. MS (ESI): $m/z$ calcd for $C_{24}H_{32}N_3O_3S$ $[M + H]^+$ 442.60; found, 442.41. $T_R$ = 19,37 min.

*(S)-2-((4-Aminophenyl)sulfonamido)-N-(1,2,3,5,6,7-hexahydro-s-indacen-4-yl)-2-phenylacetamide (**7f**).* White solid (72% yield); mp 185−187 °C. $^1$H NMR (400 MHz, DMSO-$d_6$): $\delta$ 9.58 (s, 1H), 8.19−8.02 (m, 1H), 7.47−7.42 (m, 4H), 7.38−7.21 (m, 3H), 6.90 (s, 1H), 6.58−6.48 (m, 2H), 5.88 (s, 2H), 5.11−5.08 (m, 1H), 2.74 (t, $J$ = 7.3 Hz, 4H), 2.41−2.25 (m, 4H), 1.95−1.78 (m, 4H). $^{13}$C NMR (DMSO-$d_6$): $\delta$ 167.23, 152.36, 142.65, 138.40, 137.13, 128.81, 128.30, 127.97, 127.40, 126.88, 126.00, 125.95, 117.76, 112.27, 59.24, 32.22, 29.81, 24.96. MS (ESI): $m/z$ calcd for $C_{26}H_{28}N_3O_3S$ $[M + H]^+$ 462.55; found 462.55. $T_R$ = 25,65 min.

*(S)-2-((4-Aminophenyl)sulfonamido)-N-(1,2,3,5,6,7-hexahydro-s-indacen-4-yl)-3-phenylpropanamide (**7g**).* White solid (86% yield); mp 188−189 °C. $^1$H NMR (400 MHz, DMSO-$d_6$): $\delta$ 9.38 (s, 1H), 7.65−7.61 (m, 1H), 7.32−7.20 (m, 7H), 6.90 (s, 1H), 6.48 (d, $J$ = 8.7 Hz, 2H), 5.86 (s, 2H), 4.09−4.05 (m, 1H), 2.87−2.83 (m, 2H), 2.78−2.73 (m, 4H), 2.49−2.40 (m, 4H), 1.91−1.87 (m, 4H). $^{13}$C NMR (DMSO-$d_6$): $\delta$ 168.45, 152.22, 142.55, 137.19, 136.99, 129.24, 128.98, 128.16, 127.86, 126.30, 126.15, 117.61, 112.28, 57.17, 32.29, 29.95, 25.00. MS (ESI): $m/z$ calcd for $C_{27}H_{30}N_3O_3S$ $[M + H]^+$ 476.61; found 476.59. $T_R$ = 20.75 min.

*(R)-2-((4-Aminophenyl)sulfonamido)-N-(1,2,3,5,6,7-hexahydro-s-indacen-4-yl)-3-phenylpropanamide (**7h**).* White solid (79% yield); mp 190−191 °C. $^1$H NMR (400 MHz, DMSO-$d_6$): $\delta$ 9.38 (s, 1H), 7.93 (s, 1H), 7.29 (d, $J$ = 8.7 Hz, 2H), 7.25−7.16 (m, 5H), 6.89 (s, 1H), 6.47 (d, $J$ = 8.7 Hz, 2H), 5.83 (s, 2H), 4.09 (t, $J$ = 7.3 Hz, 1H), 2.76−2.72 (m, 5H), 2.45−2.30 (m, 5H), 1.91−1.84 (m, 4H). $^{13}$C NMR (DMSO-$d_6$): $\delta$ 168.47, 152.21, 142.54, 137.20, 129.24, 128.16, 127.86, 126.14, 117.60, 112.28, 57.21, 32.29, 29.95, 25.01. MS (ESI): $m/z$ calcd for $C_{27}H_{30}N_3O_3S$ $[M + H]^+$ 476.61; found 476.27. $T_R$ = 20.22 min.

*(S)-2-((4-Aminophenyl)sulfonamido)-N-(1,2,3,5,6,7-hexahydro-s-indacen-4-yl)-3-(4-hydroxyphenyl)propanamide (**10**).* Pale yellow solid (70% yield); mp 190−192 °C. $^1$H NMR (400 MHz, DMSO-$d_6$): $\delta$ 9.27 (s, 1H), 7.50 (d, $J$ = 9.1 Hz, 1H), 7.36−7.28 (m, 2H), 6.98−6.91 (m, 2H), 6.88 (s, 1H), 6.65−6.57 (m, 2H), 6.53−6.45 (m, 2H), 4.04−3.98 (m, 1H), 2.76 (t, $J$ = 7.1 Hz, 5H), 2.67−2.52 (m, 2H), 2.45−2.29 (m, 4H), 1.95−1.84 (m, 4H). $^{13}$C NMR (DMSO-$d_6$): $\delta$ 169.10, 156.37, 152.73, 143.09, 137.77, 130.73, 129.60, 128.78, 127.55, 127.06, 118.14, 115.22, 112.90, 58.04, 32.88, 30.55, 25.60. MS (ESI): $m/z$ calcd for $C_{27}H_{30}N_3O_4S$ $[M + H]^+$ 492.61; found, 492.68. $T_R$ = 18,38 min.

*(S)-6-Amino-2-((4-aminophenyl)sulfonamido)-N-(1,2,3,5,6,7-hexahydro-s-indacen-4-yl)hexanamide (**11**).* White solid (91% yield); mp 196−197 °C. $^1$H NMR (400 MHz, DMSO-$d_6$): $\delta$ 9.29 (s, 1H), 7.64 (s, 3H), 7.42 (d, $J$ = 8.7 Hz, 2H), 7.37 (d, $J$ = 8.4 Hz, 1H), 6.92 (s, 1H), 6.55 (d, $J$ = 8.7 Hz, 2H), 3.85−3.74 (m, 1H), 2.80−2.72 (m, 6H), 2.67−2.62 (m, 1H), 2.48−2.42 (m, 4H), 2.01−1.89 (m, 4H), 1.69−1.21 (m, 5H). $^{13}$C NMR (DMSO-$d_6$): $\delta$ 168.91, 152.44, 142.66, 137.22, 128.99, 128.32, 127.67, 125.86, 117.77, 112.36, 55.66, 33.05, 32.31, 30.06, 28.91, 26.51, 25.02, 21.96. MS (ESI): $m/z$ calcd for $C_{24}H_{33}N_4O_3S$ $[M + H]^+$ 457.61; found 457.40. $T_R$ = 15,42 min.

*3-((4-Aminophenyl)sulfonamido)-N-(1,2,3,5,6,7-hexahydro-s-indacen-4-yl)propanamide (**7k**).* White solid (77% yield); mp 128−129 °C. $^1$H NMR (400 MHz, DMSO-$d_6$): $\delta$ 10.15 (s, 1H), 8.24 (d, $J$ = 8.7 Hz, 2H), 7.95 (t, $J$ = 5.8 Hz, 1H), 7.74 (s, 1H), 7.45−7.41 (m, 2H), 6.74 (s, 2H), 3.76−3.70 (m, 2H), 3.60 (t, $J$ = 7.3 Hz, 4H), 3.44 (t, $J$ = 7.3 Hz, 4H), 3.25 (t, $J$ = 7.4 Hz, 2H), 2.79−2.72 (m, 4H). $^{13}$C NMR (DMSO-$d_6$): $\delta$ 167.73, 152.38, 142.57, 137.20, 129.54, 128.35, 124.93, 117.56, 112.52, 35.43, 32.33, 30.21, 24.93. MS (ESI): $m/z$ calcd for $C_{21}H_{26}N_3O_3S$ $[M + H]^+$ 400.52; found 400.37. $T_R$ = 19,95 min.

*1-((4-Aminophenyl)sulfonyl)-N-(1,2,3,5,6,7-hexahydro-s-indacen-4-yl)pyrrolidine-2-carboxamide (**7l**).* White solid (84% yield); mp 178−179 °C. $^1$H NMR (400 MHz, DMSO-$d_6$): $\delta$ 9.25 (s, 1H), 7.49 (d, $J$ = 8.7 Hz, 2H), 6.95 (s, 1H), 6.64 (d, $J$ = 8.8 Hz, 2H), 6.05 (s, 2H), 4.02−3.99 (m, 1H), 3.47−3.39 (m, 1H), 3.14−3.04 (m, 1H), 2.80 (t, $J$ = 7.2 Hz, 4H), 2.67 (t, $J$ = 7.3 Hz, 4H), 2.01−1.90 (m, 4H), 1.88−1.74 (m, 3H), 1.58−1.48 (m, 1H). $^{13}$C NMR (DMSO-$d_6$): $\delta$ 170.15, 153.69, 143.20, 138.21, 129.86, 121.74, 118.39, 113.25, 62.16, 49.62, 32.93, 31.64, 30.55, 25.55, 24.71. MS (ESI): $m/z$ calcd for $C_{23}H_{28}N_3O_3S$ $[M + H]^+$ 426.55; found, 426.29. $T_R$ = 21,07 min.

*1-((4-Aminophenyl)sulfonyl)-N-(1,2,3,5,6,7-hexahydro-s-indacen-4-yl)piperidine-2-carboxamide (**7m**).* Pale yellow solid (71% yield); mp 99−100 °C. $^1$H NMR (400 MHz, DMSO-$d_6$): $\delta$ 9.25 (s, 1H), 7.48−7.32 (m, 2H), 6.93 (s, 1H), 6.61−6.48 (m, 2H), 4.54 (d, $J$ = 4.1 Hz, 1H), 3.64−3.56 (m, 1H), 3.47 (td, $J$ = 12.7, 2.5 Hz, 1H), 2.79 (t, $J$ = 7.3 Hz, 4H), 2.69−2.52 (m, 4H), 2.04−1.89 (m, 5H), 1.61−1.47 (m, 3H), 1.45−1.18 (m, 2H). $^{13}$C NMR (DMSO-$d_6$): $\delta$ 168.90, 153.03, 143.26, 137.88, 129.80, 129.16, 125.31, 118.32, 113.16, 54.69, 42.71, 32.91, 30.70, 28.33, 25.51, 24.37, 19.74. MS (ESI): $m/z$ calcd for $C_{24}H_{30}N_3O_3S$ $[M + H]^+$ 440.58; found, 440.37. $T_R$ = 19,58 min.

*(S)-2-((4-Aminophenyl)sulfonyl)-N-(1,2,3,5,6,7-hexahydro-s-indacen-4-yl)-1,2,3,4-tetrahydroisoquinoline-3-carboxamide (**7n**).* White solid (82% yield); mp 97−99 °C. $^1$H NMR (400 MHz,


https://doi.org/10.1021/acs.jmedchem.3c00175
J. Med. Chem. XXXX, XXX, XXX−XXX

DMSO-$d_6$): $\delta$ 9.24 (s, 1H), 7.49−7.39 (m, 2H), 7.21−7.05 (m, 4H), 6.89 (s, 1H), 6.58−6.48 (m, 2H), 4.63−4.53 (m, 2H), 4.40 (d, $J$ = 15.1 Hz, 1H), 3.04 (dd, $J$ = 15.6, 4.1 Hz, 1H), 2.85 (dd, $J$ = 15.6, 6.2 Hz, 1H), 2.74 (t, $J$ = 7.3 Hz, 4H), 2.46−2.33 (m, 4H), 1.93−1.80 (m, 4H). $^{13}$C NMR (DMSO-$d_6$): $\delta$ 168.88, 153.40, 143.12, 138.03, 133.56, 132.84, 129.61, 128.26, 127.17, 126.78, 126.59, 123.27, 118.31, 113.19, 55.39, 45.70, 32.86, 32.46, 30.36, 25.46. MS (ESI): $m/z$ calcd for $C_{28}H_{30}N_3O_3S$ $[M + H]^+$ 488.63; found, 488.63. $T_R$ = 26.22 min.

**Molecular Modeling.** *System Preparation.* The cryo-EM structure of the inactive human (h) NLPR3 (hNLPR3) in complex with ADP and NEK7 (Protein Data Bank PDB[30] ID: 6NPY[31]) was preprocessed as follows: residues upstream (from D135) and downstream (up to I655) the NACHT domain were retained, whereas the leucine-rich repeat (LRR) domains and the bound NEK7 protein were removed. Engineered residues in the cryo-EM construct were reverted to the WT sequence (UniProt[32] ID: Q96P20), and missing side chains and loops were modeled with MOE (Molecular Operating Environment (MOE), 2020.09; Chemical Computing Group ULC, 1010 Sherbooke St. West, Suite #910, Montreal, QC, Canada, H3A 2R7, 2021) using default settings: the template and target sequences were aligned with Protein Align algorithm and up to 10 models were generated by retaining the bound ADP structure during the procedure. The model returning the best GB/VI score was prepared for docking with Protonate3D.[33] Putative binding cavities were identified via the Site Finder module as implemented in MOE and the residues surrounding *Site 3* (Figure S1)—corresponding to MCC950 binding site (Figure S2) as reported in the description of the Cryo-EM structure that was not released at the time we performed the analysis and is now available[25] (PDB ID: 7PZC)—were selected for subsequent docking calculations.

*Docking & Data Analysis.* Selected compounds including the reference analogue MCC950 were docked at *Site 3* with MOE Dock: Up to 30 poses were generated with the Triangle Matcher placement method and subsequently refined via the Induced Fit procedure by saving up to 5 poses for each analogue. Pose selection was based on expected site occupancy and ligand−protein interaction patterns rather than the docking score. Hence, poses with extensive ligand−protein contacts and orientation consistent with the SAR were prioritized. A consensus binding mode for the analogues was selected based on the best consensus pose of the most active compounds with % inhibition > 55%, namely, **6c**, **7c**, **7n**, and **10**. Modeling pictures were generated with PyMOL Open Source v. 2.5.0 (The PyMOL Molecular Graphics System, Schrödinger, LLC) and protein−ligand interactions detected with PLIP.[34]

**Surface Plasmon Resonance (SPR) Experiment.** The binding of compound **10** to NLRP3 was confirmed by Surface Plasmon Resonance (SPR). The experiment was performed on a Biacore 3000 instrument (GE Healthcare/Cytiva). Recombinant NLRP3 protein (purchased from Antibodies Online, Cat. No. ABIN696430) was covalently coupled as target ligand at a high surface density of 5540 response units (RU) to flow cell 2 (FC2) of a Biacore CM5 optical sensor chip, using and following the protocol of the Biacore amine coupling kit. Amine-activated flow cell 1 (FC1) of the sensor chip was used as a reference to allow generation of a background-subtracted binding sensorgram. For analyte preparation, compound **10** was dissolved in dimethyl sulfoxide (DMSO) to generate a 40 mM stock solution which was then further diluted 1:20 in Biacore HBS-EP buffer (0.1 M HEPES, 1.5 M NaCl, 0.03 M EDTA and 0.5% v/v Surfactant P20) containing 5% DMSO. The solution was centrifuged to remove precipitated debris and then further diluted 1:1 in HBS-EP/5% DMSO. The final analyte solution (exact concentration not known due to precipitated material) was then passed over the NLRP3 ligand on the optical sensor chip at a flow rate of 30$\mu$l/min. Running buffer was HBS-EP/5% DMSO. A zero analyte concentration sensorgram was also prepared in order to allow generation of buffer subtracted curves. After the binding experiments bound analyte protein was removed by surface regeneration with 10 mM HCl.

**Pharmacology.** *Cell Culture.* Bone marrow-derived macrophages (BMDMs) were isolated from C57BL/6 mice as described[35] and differentiated for 7 days in Iscove's modified Dulbecco's medium (IMDM) supplemented with 15% fetal bovine serum (FBS, Gibco), 1% penicillin/streptomycin (P/S), and 10 ng/ml M-CSF, peritoneal macrophages were isolated as described[36] in IMDM supplemented with 15% FBS, 1% glutamine and 1% P/S, B16-F10 melanoma cells, and human THP-1 cells were grown in RPMI medium supplemented with 10% FBS, 100 U/mL penicillin, and 100 mg/mL streptomycin. THP-1 cells were stimulated by 100 ng/mL PMA overnight to differentiate into macrophages. All cells were grown in a 5% $CO_2$ incubator at 37 °C and tested with a Mycoplasma PCR Detection Kit from Sigma (MP0035-1KT).

*Inflammasome Stimulation.* Human THP-1 cells were seeded at 3 × $10^5$ cells per well in 24-well plates. The following day, the overnight medium was replaced and cells were stimulated with LPS from *Escherichia coli* 055:B5 (1 $\mu$g/mL) for 3 h. The medium was removed and replaced with serum-free medium containing DMSO or compounds (1−1000 nM) for 30 min. Cells were then stimulated with the following inflammasome activators: 5 mM adenosine 5′-triphosphate disodium salt hydrate (ATP) (1 h) or 100 $\mu$M 2′(3′)-O-(4-Benzoylbenzoyl)adenosine 5′-triphosphate (Bz-ATP) (30 min).

BMDMs were seeded at 5 × $10^5$ in 24-well plates. After 12 h, the medium was removed and cells were treated with LPS (1 $\mu$g/mL) in fresh Iscove's modified Dulbecco's medium for 2 h. After that, the medium was removed and replaced with a serum-free medium containing DMSO or compounds (1−1000 nM) for 30 min. Cells were then stimulated with the following inflammasome activators: 5 mM ATP (1 h) or 100 $\mu$M Bz-ATP (30 min).

For induction of AIM2/NLRC4 inflammasome activation, BMDMs were treated with LPS (100 ng/mL). After 3 h, the medium was removed and replaced with serum-free media containing different compounds (1 $\mu$M for 30 min); then, the cells were stimulated with poly(deoxyadenylicthymidylic) acid sodium salt (Poly dA:dT) (1 $\mu$g/mL) transfected with lipofectamine 2000 for 4 h or flagellin (100 ng/ml) from *S. typhimurium* for 2h.

*ELISA.* Supernatants from BMDMs and THP-1 cell culture were assayed for mouse or human IL-1$\beta$ (R&DSystems), mouse IL-18 (MBL International Corporation), and human IL-18 (Invitrogen), according to the manufacturer's instructions.

*Cell Viability Assay.* Cell viability was evaluated on THP-1 cells by using RealTime-Glo MT Cell Viability Assay (Promega Italia, MI). Briefly, cells were plated into 96-well opaque-walled assay plates (10 × $10^4$ cells/well), treated with selected inhibitors, and incubated for 48h. After treatment, the cells were incubated for 10 min in the cell culture incubator with a RealTime-Glo reagent according to the manufacturer's protocol. Luminescence was then measured on a Glomax Multi Detection System Promega with an integration time of 0.5 s per well every 12 h. The luminescent signal correlates with the number of metabolically active cells. Results are provided as means of luminescence values (RLU) ± SEM.

*Cell Proliferation.* B16-F10 cells were treated with selected inhibitors (1 $\mu$M) and then counted with a Burker chamber and plated in five sets of four wells of a 24-well plate. Starting from the following day (day 1), one set of wells (at days 2, 3, 4, and 5) were washed once with PBS, fixed in 4% formaldehyde solution for 15 min at room temperature, and then kept in PBS at 4°C. At day 5, all of the wells were stained with crystal violet. After lysis with 10% acetic acid, the absorbance was read at 595 nm.

*Co-Culture Assay.* Co-culture of peritoneal macrophages and B16-F10 cells was performed using Transwell chambers with 0.4 $\mu$m pores on the membranes (Corning, Corning, NY) in a 24-well plate. Peritoneal macrophages and B16-F10 cells were cultured in the lower and upper compartments of the Transwell chamber, respectively, for 48 h. Peritoneal macrophages were seeded at a density of 2 × $10^5$ cells in complete IMDM and treated with LPS (1 $\mu$g/mL) for 2 h, then DMSO or compounds (1 $\mu$M) for 30 min, and finally stimulated with ATP for 1 h. B16-F10 cells were seeded at a density of 2 × $10^3$ cells in 0.5 ml of medium. After 48 h, B16-F10 cells in the upper chambers were removed and counted using an automated cell counter (Tali image-based cytometer (Invitrogen)) according to the manufacturer's instructions.

*Western Blotting.* Human THP-1 cells were seeded at 1 × $10^6$ cells per well in six-well plates. The following day, the overnight medium was


https://doi.org/10.1021/acs.jmedchem.3c00175
J. Med. Chem. XXXX, XXX, XXX−XXX

replaced and cells were stimulated with LPS from *Escherichia coli* 055:B5 (1 $\mu$g/mL) for 3 h. The medium was removed and replaced with serum-free medium containing DMSO or compounds (1 $\mu$M) for 30 min. The cells were then stimulated with 5 mM ATP (1 h). Total cell lysates were prepared in RIPA buffer (50 mM Tris-HCl pH 7.8, 150 mM NaCl, 1% IGEPAL CA-630, 0.5% sodium deoxycholate, 0.1% SDS, 1 mM dithiothreitol (DTT)) supplemented with proteases and phosphatases inhibitors. Supernatant from THP-1 was concentrated using Pierce Protein Concentrators PES 10K MWCO (Thermo Fisher) and then centrifugated at 4000*g* for 15 min. A total of 20 $\mu$g of protein or a total of 10 $\mu$L of concentrated medium was separated by SDS-PAGE and transferred to nitrocellulose membranes for standard western blotting. The following primary antibodies were used: NLRP3 (Adipogen, #AG-20B-0014-C100), ASC (Adipogen, #AG-20B-0014-C100) Caspase 1 (Novus Biological, #14F468) IL-1$\beta$ (Cell Signaling Technology, #12242), GAPDH (Cell Signaling Technology, #2118), and $\beta$-Actin (Sigma, #A2668). Isotype-matched horseradish peroxidase-conjugated secondary antibodies were used, followed by detection using chemiluminescence (GE Image-Quant).

*Co-Immunoprecipitation.* After treatment with LPS, compounds, and ATP, BMDMs ($1 \times 10^7$) were collected and lysed with IP lysis buffer containing 50 mM HEPES, 150 mM NaCl, 10% glycerol 2 mM EDTA, and 0.5% Tryton and supplemented with a proteases inhibitor mixture and Phos-STOP Phosphatase Inhibitor Cocktail (Roche Applied Science). The same amount of extracted proteins for each condition was incubated O/N with the specific primary antibody ASC (Adipogen, #AG-20B-0014-C100). The immunocomplexes were captured with the appropriate dynabeads (Thermo Fisher) in accordance with the manufacturer's instructions. Beads were pelleted and washed three times. The bait was eluted in Laemmli sample buffer and denatured for 5 min at 100 °C. Samples were proceeded by SDS-PAGE and analyzed by standard (WB) blotting technique.

*ASC Oligomerization Assay.* A total of $1 \times 10^7$ BMDMs were cultured in complete IMDM. The next day, the O/N medium was replaced, and the cells were stimulated with LPS (1 $\mu$g/mL) for 2 h, DMSO, or compounds (1 $\mu$M) for 30 min and then with 5 mM ATP (1 h). The supernatants were removed, the cells were rinsed in ice-cold PBS and 1 mL of ice-cold buffer (20 mM HEPES-KOH, pH 7.5, 150 mM KCL, 1% NP-40, 0.1 mM PMSF, 1 mg/ml leupeptin, 11.5 mg/ml aprotinin, and 1 mM sodium orthovanadate) was added. The cells were scraped and lysed by being sheared 10 times through a 21-gauge needle. 50 $\mu$L of lysate was removed for western blot analysis. Lysates were centrifuged at 330*g* for 10 min at 4 °C. The pellets were washed twice in 1 ml of ice-cold PBS and resuspended in 500 $\mu$L of PBS. 2 mM Disuccinimydyl suberate (DSS) (from a fresh 100 mM stock prepared from DSS equilibrated to room temperature and made up in dry DMSO) was added to the resuspended pellets, which were incubated at room temperature for 30 min with rotation. Samples were then centrifuged at 330*g* for 10 min at 4 °C. The supernatant was removed, and the cross-linked pellets were resuspended in 30 $\mu$L of Laemmli sample buffer. Samples were boiled for 5 min at 99 °C and analyzed by western blotting.

*Immunofluorescence.* BMDMs cultured in complete IMDM and treated as described above were fixed with 4% paraformaldehyde (PFA) in PBS for 10 min and washed three times with PBS. The cells were permeabilized for 10 min with 0.1% Triton X-100 in PBS and blocked with PBS containing 5% BSA and 0.1% Triton X-100 for 1 h. Cells were incubated O/N at 4 °C with rabbit anti-AS (1:100). After washing with PBS three times, the cells were incubated with AlexaFluor-conjugated secondary antibodies (diluted 1:1000, Life Technologies goat anti-rabbit 594). Nuclei were stained with Hoechts (1 $\mu$M) for 30 min and washed with PBS three times. The coverslips were mounted with ProLong Gold Antifade reagent (Life Technologies), and immunofluorescence analysis was performed with a confocal laser scanner microscope (Olympus FV3000) equipped with a 63× oil objective.

*In Vivo LPS Challenge.* C57BL/6 mice were IP injected with inhibitors (25 mg/kg) or vehicle control (DMSO) 30 min before IP injection of LPS 1 mg/kg (4 h) and then were euthanized and blood and peritoneal exudate were isolated. Mouse plasma was collected after blood centrifugation (1000*g*, 15 min at 4 °C). ELISA for IL-1$\beta$ was performed according to the manufacturer's instructions (R&DSystems).

*Tumor Generation and In Vivo Drug Administration.* Procedures involving animals and their care were in conformity with institutional guidelines, and Animal Ethics Committee approved all experimental protocols (Authorization No. 481/2017-PR and CBCC2.N.BH4 approved by Italian Ministry of Health). All mice were housed in a temperature-controlled environment with 12 h light/dark cycles and received food and water ad libitum. A total of $1 \times 10^6$ B16-F10 melanoma cells transfected with cytluc (B16-F10cytLUC) were subcutaneously inoculated into females, 6- to 8-week-old C57BL/6 mice. Tumor growth was monitored daily, and tumor volumes were measured every other day with calipers using the following equation: Volume = $\pi/6 \times (a \times b2)$, where "*a*" is the major diameter and "*b*" is the minor diameter. The mice were randomly divided into treatment groups and the control group, with five mice per group. For NLRP3 inflammasome inhibition, the mice were IP injected with selected molecules thrice weekly at 25 mg/kg; control mice received equal volumes of DMSO. Luciferase luminescence was followed with a total body luminometer (IVIS Lumina, Caliper-PerkinElmer). Briefly, the mice were anesthetized with 2.5% isofluorane IP injected with 150 mg/kg D-luciferin (Promega) and luminescence was quantified after 15 min using the Living Image Software (Caliper). All of the mice that reached the endpoint of the experiment were euthanized and, subsequently, tumors were excised and weighed. Excised tumor masses were homogenized in lysis buffer (300 mmol/L sucrose, 1 mmol/L $K_2HPO_4$, 5.5 mmol/L D-glucose, 20 mmol/L Hepes, 1mmol/L phenylmethylsulfonyl fluoride, 1 mmol/L benzamidine, 0.5% IGEPAL) with an electric homogenizer. Lysates were assayed for western blot analysis.

***In Vitro* Oxidative Metabolic Stability in Hepatic Microsomes.** *Intrinsic clearance in microsomes*:[37] mouse (Sigma-Aldrich, CD-1 male, pooled) and human microsomes (Sigma-Aldrich, human, pooled) were preincubated at 0.5 mg/mL with the test compound dissolved in DMSO at 1 $\mu$M in phosphate buffer 50 mM, pH 7.4, and 3 mM $MgCl_2$ for 10 min at 37 °C. The reaction was then started by adding the cofactor mixture solution (NADP, glucose-6-phosphate, glucose-6-phosphate dehydrogenase in 2% $NaHCO_3$). Samples were taken at 0, 10, 30, 45, and 60 min and added to acetonitrile to stop the reaction. Samples were then centrifuged, and the supernatant was analyzed by LC-MS/MS to quantify the amount of compound. A control sample without cofactor was always added to check the chemical stability of the test compound. Two reference compounds of known metabolic stability, 7-EC and propranolol, were present in parallel testing. A fixed concentration of diclofenac was added in every sample as an internal standard for LC-MS/MS analyses. The percentage of the area of the test compound remaining at the various incubation times was calculated with respect to the area of the compound at time 0 min. The intrinsic clearance (Cli) was calculated by the equation

$$\text{Cli}(\mu\text{L/min /mg}) = k/\text{microsomal conc.} \times 1000$$

where $k$ is the rate constant ($\text{min}^{-1}$); microsomal protein conc. = 0.5 mg protein/mL. The rate constant, $k$ ($\text{min}^{-1}$) derived for the exponential decay equation (peak area/IS vs time) was used to calculate the rate of Cli. Classification of in vitro stability is presented in Table S1 (Supporting Information).

*LC−MS/MS analytical method*: samples were analyzed under the following conditions: UPLC Waters coupled with an API 3200 triple-quadrupole (ABSciex); eluents, (phase A) 95% water, 5% acetonitrile + 0.1% HCOOH, (phase B) 5% water, 95% acetonitrile + 0.1% HCOOH; flow rate, 0.3 mL/min; column, Gemini-Nx 5 $\mu$m C18 110A (50 × 2.00 $\text{mm}^2$) at 35 °C; injection volume, 10 $\mu$L. LC−MS/MS analyses were carried out using an ESI(±) interface in multiple reaction monitoring (MRM) mode. Conditions and MRM transitions applied to the compounds are described in Table S2 (Supporting Information). Source conditions ESI positive/negative: T 450 °C, Gas 1 45, Gas 2 40, CUR 20, IS 5500 (or −4500 for compound **6c**), CAD 5.

***In Vivo* Pharmacokinetics.** 8-Week-old healthy female C57BL/6 mice (25−30 g of body weight) were housed under a 12 h light/dark cycle in a controlled environment (22 ± 2 °C with a relative humidity of


https://doi.org/10.1021/acs.jmedchem.3c00175
J. Med. Chem. XXXX, XXX, XXX−XXX

55 ± 10%) in the institutional animal facility with ad libitum access to food and water. Procedures involving animals, and their care were in conformity with institutional guidelines, and Animal Ethics Committee approved all experimental protocols (Authorization No. 481/2017-PR approved by Italian Ministry of Health). Compound **6c** (25 mg/kg) was administered by IP injection ($n$ = 24, 3 mice/time point). The mice were sacrificed at different time points, i.e., 5, 20 min, 1, 2, 3, 6, 8, and 24 h after the injection and blood was collected from the cava vein in tubes coated with Li-heparin anticoagulant and centrifuged at +4 °C, 3000$g$ for 10 min to obtain the plasma. Samples were analyzed for their compound **6c** content using the LC-MS/MS method. Stock solution of compound **6c** and diclofenac used as internal standard were prepared in ACN at 1 mg/mL. Working solutions for the calibration curves and QC samples were prepared by sequential dilution in ACN.

45 μL of blank plasma was added to 200 μL of ACN/MeOH 1:1 containing diclofenac at 25 ng/mL as internal standards. Samples were vortexed for 3 min and centrifuged for 15 min at 5 °C at 4600 rpm. Samples were transferred into a 96-well plate and analyzed on a UPLC Acquity (Waters, Milford, MA) coupled with an API 3200 Triple Quadrupole (ABSciex). Mobile phases were: (phase A) 95% water, 5% acetonitrile + 0.1% HCOOH, (phase B) 5% water, 95% acetonitrile + 0.1% HCOOH; flow rate, 0.3 mL/min; column, Gemini-Nx 5 μm C18 110A (50 × 2.00 $mm^2$) at 35 °C; injection volume, 10 μL. The retention time for compound **6c** is 2.26 min.

MS/MS analyses were carried out using an ESI(-) interface in multiple reaction monitoring (MRM) mode. Conditions and MRM transitions applied to the compounds are described in Table S2. Compound **6c** analytical range in plasma was 1−2000 ng/mL; pharmacokinetic parameters were calculated using Excel add-in.[38] AUCs were calculated using an NCA by the linear trapezoidal rule, and a uniform weight was performed as a first approach. Graphical concentration−time curves were produced after Log transformation. The ke was estimated from the terminal part of the log-concentration−time plot including at least three data points excluding the $C_{max}$.

*Statistical Analysis.* The data were analyzed by Prism 7 (GraphPad). Unless otherwise noted in figure legends, data are representative of at least three biologically independent experiments. Two-group datasets were analyzed by Student's unpaired $t$-test. For three or more group analyses, one-way ANOVA Tukey's multiple comparison test was used. One asterisk was used for $p < 0.05$, two for $p < 0.01$, three for $p < 0.001$, and four for $p < 0.0001$.

## ■ ASSOCIATED CONTENT

### Supporting Information

The Supporting Information is available free of charge at https://pubs.acs.org/doi/10.1021/acs.jmedchem.3c00175.

Three-dimensional coordinates of hNLRP3 homology model used for docking (PDB)

Predicted and experimental MCC950 binding site and pose comparison (Figure S1), predicted binding mode of compound **7n** (Figure S2), HPLC chromatograms, ESI mass spectra, $^{1}$H NMR and $^{13}$C NMR, and IR spectra of the final compounds, HRMS of the final compounds (Figures S3−S5), in vitro clearance classification (Table S1), and compound MRM transition and conditions (Table S2) (PDF)

Molecular formula strings (CSV)

## ■ AUTHOR INFORMATION


### Corresponding Authors

**Delia Preti** − *Department of Chemical, Pharmaceutical and Agricultural Sciences, University of Ferrara, 44121 Ferrara, Italy;* orcid.org/0000-0002-1075-3781; Email: prtdle@unife.it

**Carlotta Giorgi** − *Department of Medical Sciences, Section of Experimental Medicine, University of Ferrara, 44121 Ferrara, Italy; Technopole of Ferrara, Laboratory for Advanced Therapies (LTTA), 44121 Ferrara, Italy;* orcid.org/0000-0002-2494-7405; Email: grgclt@unife.it

### Authors

**Valentina Albanese** − *Department of Environmental and Prevention Sciences, University of Ferrara, 44121 Ferrara, Italy;* orcid.org/0000-0002-1947-2644

**Sonia Missiroli** − *Department of Medical Sciences, Section of Experimental Medicine, University of Ferrara, 44121 Ferrara, Italy; Technopole of Ferrara, Laboratory for Advanced Therapies (LTTA), 44121 Ferrara, Italy*

**Mariasole Perrone** − *Department of Medical Sciences, Section of Experimental Medicine, University of Ferrara, 44121 Ferrara, Italy; Technopole of Ferrara, Laboratory for Advanced Therapies (LTTA), 44121 Ferrara, Italy*

**Martina Fabbri** − *Department of Chemical, Pharmaceutical and Agricultural Sciences, University of Ferrara, 44121 Ferrara, Italy*

**Caterina Boncompagni** − *Department of Medical Sciences, Section of Experimental Medicine, University of Ferrara, 44121 Ferrara, Italy; Technopole of Ferrara, Laboratory for Advanced Therapies (LTTA), 44121 Ferrara, Italy*

**Salvatore Pacifico** − *Department of Chemical, Pharmaceutical and Agricultural Sciences, University of Ferrara, 44121 Ferrara, Italy;* orcid.org/0000-0002-3377-5107

**Tiziano De Ventura** − *Department of Chemical, Pharmaceutical and Agricultural Sciences, University of Ferrara, 44121 Ferrara, Italy*

**Antonella Ciancetta** − *Department of Chemical, Pharmaceutical and Agricultural Sciences, University of Ferrara, 44121 Ferrara, Italy;* orcid.org/0000-0002-7612-2050

**Giulio Dondio** − *Aphad Srl, 20090 Buccinasco, Italy*

**Franz Kricek** − *NBS-C Bioscience & Consulting GmbH, 1230 Vienna, Austria*

**Paolo Pinton** − *Department of Medical Sciences, Section of Experimental Medicine, University of Ferrara, 44121 Ferrara, Italy; Technopole of Ferrara, Laboratory for Advanced Therapies (LTTA), 44121 Ferrara, Italy;* orcid.org/0000-0001-7108-6508

**Remo Guerrini** − *Technopole of Ferrara, Laboratory for Advanced Therapies (LTTA), 44121 Ferrara, Italy; Department of Chemical, Pharmaceutical and Agricultural Sciences, University of Ferrara, 44121 Ferrara, Italy*

Complete contact information is available at: https://pubs.acs.org/10.1021/acs.jmedchem.3c00175


### Author Contributions

[▽]V.A., S.M., and M.P. contributed equally to the work. All authors have given approval for the final version of the manuscript.

### Notes

The authors declare no competing financial interest.

S.P., V.A., D.P., S.M., P.P., C.G., and M.P. are inventors of the patent applications (nos. 102022000008246; 102022000008294; 102022000008321) focused on NLRP3 inhibitors.

## ■ ACKNOWLEDGMENTS

The Signal Transduction Laboratory was supported by the Italian Association for Cancer Research (AIRC, IG-23670 to

P.P. and IG-19803 to C.G.), A-ROSE, Progetti di Rilevante Interesse Nazionale (PRIN2017E5L5P3 to P.P and PRIN20177E9EPY to C.G.), the Italian Ministry of Health (GR-2013-02356747 to C.G., GR-2019-12369646 to S.M. and S.P.), the European Research Council (853057-InflaPML to C.G.), and local funds from the University of Ferrara to C.G., P.P., D.P., S.P., and R.G. M.P. was supported by AIRC research fellowship (ID: 26665). P.P. is grateful to C. degli Scrovegni for her continuous support.

## ■ ABBREVIATIONS USED

ASC, adaptor apoptosis-associated speck-like protein; ASDs, aryl sulfonamide derivatives; BMDM, marrow-derived macrophages; Bz-ATP, 2′(3′)-O-(4-benzoylbenzoyl)adenosine 5′-triphosphate triethylammonium salt; CAPS, cryopyrin-associated periodic syndrome; CARD, caspase activation and recruitment domain; DAMPs, damage-associated molecular patterns; IFD, induced fit docking; IL-1$\beta$, interleukin-1$\beta$; IL-18, interleukin-18; IP, intraperitoneal; LPS, lipopolysaccharide; PAMPs, pathogen-associated molecular patterns; PYD, N-terminal pyrin domain; RT, room temperature; TLR, Toll-like receptor

## ■ REFERENCES

(1) Missiroli, S.; Patergnani, S.; Caroccia, N.; et al. Mitochondria-associated membranes (MAMs) and inflammation. *Cell Death Dis.* **2018**, *9*, 329.
(2) Paik, S.; Kim, J. K.; Silwal, P.; Sasakawa, C.; Jo, E. K. An update on the regulatory mechanisms of NLRP3 inflammasome activation. *Cell Mol. Immunol.* **2021**, *18*, 1141−1160.
(3) Swanson, K. V.; Deng, M.; Ting, J. P. The NLRP3 inflammasome: molecular activation and regulation to therapeutics. *Nat. Rev. Immunol.* **2019**, *19*, 477−489.
(4) Missiroli, S.; Perrone, M.; Boncompagni, C.; et al. Targeting the NLRP3 Inflammasome as a New Therapeutic Option for Overcoming Cancer. *Cancers* **2021**, *13*, 2297.
(5) Zhang, X.; Xu, A.; Lv, J.; et al. Development of small molecule inhibitors targeting NLRP3 inflammasome pathway for inflammatory diseases. *Eur. J. Med. Chem.* **2020**, *185*, No. 111822.
(6) Su, M.; Wang, W.; Liu, F.; Li, H. Recent Progress on the Discovery of NLRP3 Inhibitors and their Therapeutic Potential. *Curr. Med. Chem.* **2021**, *28*, 569−582.
(7) Agarwal, S.; Sasane, S.; Shah, H. A.; et al. Discovery of N-Cyano-sulfoximineurea Derivatives as Potent and Orally Bioavailable NLRP3 Inflammasome Inhibitors. *ACS Med. Chem. Lett.* **2020**, *11*, 414−418.
(8) Dai, Z.; Chen, X. y.; An, L. y.; et al. Development of Novel Tetrahydroquinoline Inhibitors of NLRP3 Inflammasome for Potential Treatment of DSS-Induced Mouse Colitis. *J. Med. Chem.* **2021**, *64*, 871−889.
(9) De Ventura, T.; Perrone, M.; Missiroli, S.; et al. Synthesis and NLRP3-Inflammasome Inhibitory Activity of the Naturally Occurring Velutone F and of Its Non-Natural Regioisomeric Chalconoids. *Int. J. Mol. Sci.* **2022**, *23*, 8957.
(10) McBride, C.; Trzoss, L.; Povero, D.; et al. Overcoming Preclinical Safety Obstacles to Discover (S)-N-((1,2,3,5,6,7-Hexahydro-s-indacen-4-yl)carbamoyl)-6-(methylamino)-6,7-dihydro-5H-pyrazolo[5,1-b][1,3]oxazine-3-sulfonamide (GDC-2394): A Potent and Selective NLRP3 Inhibitor. *J. Med. Chem.* **2022**, *65*, 14721−14739.
(11) Narros-Fernández, P.; Chioua, M.; Petcu, S. A.; et al. Synthesis and Pharmacological Evaluation of New N-Sulfonylureas as NLRP3 Inflammasome Inhibitors: Identification of a Hit Compound to Treat Gout. *J. Med. Chem.* **2022**, *65*, 6250−6260.
(12) Laliberte, R. E.; et al. Glutathione s-transferase omega 1-1 is a target of cytokine release inhibitory drugs and may be responsible for their effect on interleukin-1beta posttranslational processing. *J. Biol. Chem.* **2003**, *278*, 16567−16578.
(13) Coll, R. C.; Robertson, A. A. B.; Chae, J. J.; et al. A small-molecule inhibitor of the NLRP3 inflammasome for the treatment of inflammatory diseases. *Nat. Med.* **2015**, *21*, 248−255.
(14) Coll, R. C.; Hill, J. R.; Day, C. J.; et al. MCC950 directly targets the NLRP3 ATP-hydrolysis motif for inflammasome inhibition. *Nat. Chem. Biol.* **2019**, *15*, 556−559.
(15) Tapia-Abellán, A.; Angosto-Bazarra, D.; Martínez-Banaclocha, H.; et al. MCC950 closes the active conformation of NLRP3 to an inactive state. *Nat. Chem. Biol.* **2019**, *15*, 560−564.
(16) Mangan, M. S. J.; Olhava, E. J.; Roush, W. R.; et al. Targeting the NLRP3 inflammasome in inflammatory diseases. *Nat. Rev. Drug Discovery* **2018**, *17*, 588−606.
(17) Hamarsheh, S.; Osswald, L.; Saller, B. S.; et al. Oncogenic Kras(G12D) causes myeloproliferation via NLRP3 inflammasome activation. *Nat. Commun.* **2020**, *11*, No. 1659.
(18) Yaw, A. C. K.; Chan, E.W.L.; Yap, J.K.Y.; Mai, C. W. The effects of NLRP3 inflammasome inhibition by MCC950 on LPS-induced pancreatic adenocarcinoma inflammation. *J. Cancer Res. Clin. Oncol.* **2020**, *146*, 2219−2229.
(19) Chen, L.; Huang, C. F.; Li, Y. C.; et al. Blockage of the NLRP3 inflammasome by MCC950 improves anti-tumor immune responses in head and neck squamous cell carcinoma. *Cell. Mol. Life Sci.* **2018**, *75*, 2045−2058.
(20) Hill, J. R.; Coll, R. C.; Sue, N.; et al. Sulfonylureas as Concomitant Insulin Secretagogues and NLRP3 Inflammasome Inhibitors. *ChemMedChem* **2017**, *12*, 1449−1457.
(21) Harrison, D.; Boutard, N.; Brzozka, K.; et al. Discovery of a series of ester-substituted NLRP3 inflammasome inhibitors. *Bioorg. Med. Chem. Lett.* **2020**, *30*, No. 127560.
(22) Ashcroft, F. M.; Rorsman, P. Diabetes mellitus and the beta cell: the last ten years. *Cell* **2012**, *148*, 1160−1171.
(23) Smith, G. F. Designing Drugs to Avoid Toxicity. In *Progress in Medicinal Chemistry*, 2011; Vol. *50*, pp 1−47.
(24) Savka, R. D.; Plenio, H. A hexahydro-s-indacene based NHC ligand for olefin metathesis catalysts. *J. Organomet. Chem.* **2012**, *710*, 68−74.
(25) Hochheiser, I. V.; Pilsl, M.; Hagelueken, G.; et al. Structure of the NLRP3 decamer bound to the cytokine release inhibitor CRID3. *Nature* **2022**, *604*, 184−189.
(26) Missiroli, S.; et al. PML at mitochondria-associated membranes governs a trimeric complex with NLRP3 and P2X7R that modulates the tumor immune microenvironment. *Cell Death Differ.* **2022**, *30*, 429−441.
(27) Tengesdal, I. W.; Menon, D. R.; Osborne, D. G.; et al. Targeting tumor-derived NLRP3 reduces melanoma progression by limiting MDSCs expansion. *Proc. Natl. Acad. Sci. U.S.A.* **2021**, *118*, e2000915118.
(28) Voet, S.; Srinivasan, S.; Lamkanfi, M.; van Loo, G. Inflammasomes in neuroinflammatory and neurodegenerative diseases. *EMBO Mol. Med.* **2019**, *11*, e10248.
(29) Yang, Y.; Wang, H.; Kouadir, M.; Song, H.; Shi, F. Recent advances in the mechanisms of NLRP3 inflammasome activation and its inhibitors. *Cell Death Dis.* **2019**, *10*, 128.
(30) Bernstein, F. C.; Koetzle, T. F.; Williams, G. J. B.; et al. The Protein Data Bank. A computer-based archival file for macromolecular structures. *Eur. J. Biochem.* **1977**, *80*, 319−324.
(31) Sharif, H.; Wang, L.; Wang, W. L.; et al. Structural mechanism for NEK7-licensed activation of NLRP3 inflammasome. *Nature* **2019**, *570*, 338−343.
(32) Apweiler, R.; et al. UniProt: the Universal Protein knowledgebase. *Nucleic Acids Res.* **2004**, *32*, 115D−119.
(33) Labute, P. Protonate3D: assignment of ionization states and hydrogen coordinates to macromolecular structures. *Proteins* **2009**, *75*, 187−205.
(34) Salentin, S.; Schreiber, S.; Haupt, V. J.; Adasme, M. F.; Schroeder, M. PLIP: fully automated protein-ligand interaction profiler. *Nucleic Acids Res.* **2015**, *43*, W443−W447.


https://doi.org/10.1021/acs.jmedchem.3c00175
J. Med. Chem. XXXX, XXX, XXX−XXX

(35) Ying, W.; Cheruku, P. S.; Bazer, F. W.; Safe, S. H.; Zhou, B. Investigation of macrophage polarization using bone marrow derived macrophages. *J. Vis. Exp.* **2013**, e50323.
(36) Zhang, X.; Goncalves, R.; Mosser, D. M. The isolation and characterization of murine macrophages. *Curr. Protoc. Immunol.* **2008**, *83*, 14-1.
(37) Clarke, S. E.; Jeffrey, P. Utility of metabolic stability screening: comparison of in vitro and in vivo clearance. *Xenobiotica* **2001**, *31*, 591−598.
(38) Zhang, Y.; Huo, M.; Zhou, J.; Xie, S. PKSolver: An add-in program for pharmacokinetic and pharmacodynamic data analysis in Microsoft Excel. *Comput. Methods Programs Biomed.* **2010**, *99*, 306−314.


https://doi.org/10.1021/acs.jmedchem.3c00175
*J. Med. Chem.* XXXX, XXX, XXX−XXX